ATLANTIC MERIDIONAL OVERTURNING CIRCULATION VARIABILITY SINCE THE LAST GLACIATION: INSIGHTS FROM A NOVEL MULTIPROXY APPROACH

A Dissertation
Presented to
The Academic Faculty

by

Shannon G. Valley

In Partial Fulfillment
of the Requirements for the Degree
Doctor of Philosophy in the
School of Earth and Atmospheric Sciences

Georgia Institute of Technology
December 2019

ATLANTIC MERIDIONAL OVERTURNING CIRCULATION VARIABILITY SINCE THE LAST GLACIATION: INSIGHTS FROM A NOVEL MULTIPROXY APPROACH

Approved by:

Dr. Jean Lynch-Stieglitz, Advisor
School of Earth and Atmospheric Sciences
Georgia Institute of Technology

Dr. Annalisa Bracco
School of Earth and Atmospheric Sciences
Georgia Institute of Technology

Dr. Kim Cobb
School of Earth and Atmospheric Sciences
Georgia Institute of Technology

Dr. Thomas M. Marchitto
Department of Geological Sciences
University of Colorado Boulder

Dr. Takamitsu Ito
School of Earth and Atmospheric Sciences
Georgia Institute of Technology

Date Approved: October 9, 2019

In memory of my father, Thomas James Valley

ACKNOWLEDGEMENTS

It takes a village to make a PhD. I would like to first thank Dr. Jean Lynch-Stieglitz, who has exemplified what it means to be a great advisor: encouraging, demanding, and attuned to my specific goals and needs as a developing researcher. I am grateful for all of my committee for their guidance over the years, and especially Tom Marchitto, who has generously hosted me in his lab and also lent me his bike. I thank Tammy Chang, who taught me everthing I know about working in a lab, for her expertise and patience. Going back even further, I thank past teachers Richard Golenko, Abdi Darai, and my army of NASA colleagues and mentors, for giving me the knowledge and confidence to pursue a PhD.

Of course, I would not be here without the support and grounding of my family by birth, including my dad Tom, who foresaw this moment but did not live to see my PhD completed, my mom Carol and my sister Taylor, as well as the other Valleys, Irvings, Daughertys and Solomons. My incredible chosen family is large but I thank especially my adopted aunt Faye Hadrick, and best friends Gayla Burks and Zainab Naqvi.

My friends and colleagues Pam Grothe, Minda Monteagudo, Tyler Vollmer, Karim Lakhani, Shelby Ellis, Annika Jerslid, and Anise Grant have been so essential for helping me navigate graduate student life, liberty and pursuits of happiness, as well as providing the occaisional shoulder to cry on. In this category I especially highlight Hussein Sayani, who has been quite literally the best roommate ever. Last but certainly not least, I am grateful to Nicolò Ardenghi, who for these past years has been my partner, my heart, and my figure-making guru. Thank you.

TABLE OF CONTENTS

LIST OF TABLES

LIST OF FIGURES

LIST OF SYMBOLS AND ABBREVIATIONS

^{230}Th	Thorium-230
^{231}Pa	Protactinium-231
AAIW	Antarctic Intermediate Water
Al	Aluminum
AMO	Atlantic Multidecadal Oscillation
AMOC	Atlantic Meridional Overturning Circulation
AMV	Atlantic Multidecadal Variability
BA	Bølling-Allerød
BP	Before present
Ca	Calcium
Cd	Cadmium
Cd_w	Seawater Cadmium
CE	Common Era
$\delta^{13}C$	Ratio of carbon-13 to carbon-12
$\delta^{18}O$	Ratio of oxygen-18 to oxygen-16
$\delta^{18}Oc$	Ratio of oxygen-18 to oxygen-16 of calcite
$\delta^{18}O_W$	Ratio of oxygen-18 to oxygen-16 of seawater
D-O	Dansgaard-Oeschger
EASM	East Asian Summer Monsoon
$\boldsymbol{\varepsilon}_{Nd}$	Ratio of neodymium isotopes in a sample to neodymium isotopes in a chondrite standard
Fe	Iron
GNAIW	Glacial North Atlantic Intermediate Water
HS	Heinrich Stadial

ITCZ	Intertropical Convergence Zone
IVF	Ice volume-free
ka	Thousand calendar years ago
LGM	Last Glacial Maximum
Li	Lithium
LIA	Little Ice Age
Mg	Magnesium
MIS	Marine isotope stage
Mn	Manganese
MWP	Medieval Warm Period
NADW	North Atlantic Deep Water
PDB	PeeDee Belemnite
PO_4	Phosphate
psu	Practical salinity unit
SMOW	Standard mean ocean water
SST	Sea surface temperature
T, t	Temperature
YD	Younger Dryas

SUMMARY

Atlantic Meridional Overturning Circulation (AMOC) transports warm surface water northward across the equator, carrying heat from the Southern to the Northern Hemisphere. AMOC plays a central role in the global redistribution of heat and precipitation during both abrupt and longer-term climate shifts. Over the next century, AMOC is projected to weaken due to greenhouse gas warming, though projecting the variability of its future behavior is dependent on a better understanding of how AMOC changes are forced, including the evolving states of its constituent water masses. To address this, I analyzed several water mass tracer records from Florida Straits intermediate water- a water mass that forms part of AMOC's upper branch.

To investigate AMOC variability during the Younger Dryas (YD) and Heinrich Stadial 1 (HS1)- climatological periods associated with ice sheet melt- I generated a new, high-resolution record of benthic seawater Cd (Cd_w) from a Florida Straits sediment core at 546 m water depth. This record provides additional evidence for lower Cd_w relative to modern during both the YD and HS1. Lower Cd_w values are interpreted as AMOC weakening, reflecting a decreased northward transport of southern-sourced higher-nutrient intermediate waters by the surface return flow of AMOC. Comparison of this new Cd_w record with previously published neodymium isotope and $\delta^{18}O$ records from the same core shows synchronous transitions, further illustrating the connection between Cd_w levels and AMOC strength in the Florida Straits. An increase in Cd_w near 16 ka bolsters existing evidence for a resumption of upper branch AMOC strength approximately midway through Heinrich Stadial 1.

The Cd_w record was extended to ~35,000 yr before present, including all of Marine Isotope Stages (MIS) 2 and part of MIS 3, and temperature and oxygen isotopic composition of seawater were also reconstructed from the same core in order to provide a fuller picture of water mass properties and circulation at this location. During the Last Glacial Maximum (LGM, 19-23 kyr before present), Cd_w levels were generally low. A novel Mg/Li-derived temperature record reveals persistently cold glacial temperatures (~3.6 ℃, two to three degrees colder than during the Holocene or MIS3). My published study is one of the first to make use of this promising new temperature proxy.

In contrast to the YD and HS1, there is no indication of AMOC variability over Heinrich Stadials 2 and 3, consistent with previous studies that conclude the AMOC is less sensitive to freshwater forcing during glaciations than during the last deglaciation. While there is some inconsistency between proxies, Cd_w increases over some MIS3 Dansgaard-Oeschger interstadials, providing qualified support for a strengthening in AMOC. This study highlights the distinct nature of water masses and circulation during the LGM, relative to the stadial (weak AMOC) periods of the deglaciation and Late MIS 3.

Seeking to resolve an apparent contradiction of AMOC trends from paleorecords of the more recent past, I applied the Cd_w Florida Straits transport characterization to infer upper AMOC change over the last ~1,000 years. In combined core records from intermediate water depth with high resolution over the Common Era, there is little evidence of AMOC reduction over the Little Ice Age relative to that during the YD

stadial. Limited data since 1850 CE prohibits comparison of this record to other AMOC proxies in the modern era. However, from the Medieval Warm Period through the Little Ice Age, the newly generated Cd_w and Mg/Li-derived temperature records are consistent with other indicators of AMOC variability that were reconstructed from further north in the Atlantic. This agreement supports evidence for a meridionally consistent AMOC on decadal and greater timescales.

CHAPTER 1. TIMING OF DEGLACIAL AMOC VARIABILITY FROM A HIGH-RESOLUTION SEAWATER CADMIUM RECONSTRUCTION

(Previously published as: Valley, S., Lynch-Stieglitz, J., & Marchitto, T. M. (2017). Timing of deglacial AMOC variability from a high-resolution seawater cadmium reconstruction. Paleoceanography, 32, 1195–1203.)

1.1 Introduction

Atlantic Meridional Overturning Circulation (AMOC) in the modern ocean transports heat from the Southern to the Northern Hemisphere because the formation and southward flow of cold deep water in the North Atlantic is compensated by the northward flow of warmer water in the upper ocean. Because it transports heat, the AMOC may cause and/or play a role in the global expression of abrupt climate changes over the last glacial cycle. Reconstructions of both conservative and nonconservative water mass properties have revealed a more stratified north Atlantic during the Last Glacial Maximum (LGM) around 20 ka, with shallow overturning limited to about the top 2 km, and during certain periods of the deglaciation, little or no overturning at all (Adkins, 2013; Boyle & Keigwin, 1987; Lynch-Stieglitz et al., 2007; McManus et al., 2004; Rahmstorf, 2002). Evidence for AMOC reduction has coincided with abrupt and short-lived (millennial scale) cold periods observed in the Northern Hemisphere. These cold periods are thought to be induced by large influxes of freshwater during glacial melt and ice sheet calving (Boyle & Keigwin, 1987; Broecker, 1994; Rooth, 1982). The connection between freshwater fluxes and AMOC changes has been validated by data from circulation tracers and nutrient proxies and is supported by modeling studies, for example, Gregory et al. (2006), Kageyama et al. (2010), and Rahmstorf (1995). However,

uncertainty remains around the precise triggers, timing, and sequence of changes in AMOC.

Intermediate waters in the modern Florida Straits are composed of a mixture of waters originating in the Southern Hemisphere entering the Caribbean from the south and waters originating in the Northern Hemisphere flowing into the Caribbean as the western limb of the North Atlantic gyre (Figure 1-1, left). The two water mass inputs into the Straits differ in their nutrient content. Waters coming from the south, which form part of the upper branch of the AMOC, have high nutrient concentrations and those from the north have relatively lower nutrient concentrations.

Florida Straits reconstructed seawater cadmium (Cd_w) has been used to infer changes in the upper branch of AMOC over the Younger Dryas North Atlantic cold period (YD, 12.7–11.5 ka) (Came et al., 2008). Cadmium has a nutrient-like profile that closely resembles phosphate in the modern ocean (Boyle et al., 1976). Higher Cd_w is expected in the Florida Straits when AMOC is strong, as the enhanced circulation increases the northward influx of higher-nutrient intermediate water from farther south in the Atlantic. This study provides a higher-resolution benthic Cd_w record than previously available for the region, complete for both Heinrich Stadial 1 (HS1, 17.5–14.5 ka) and much of the YD. The new Cd_w record allows for direct comparison against other measures of circulation and nutrient changes from other proxies in the same core.

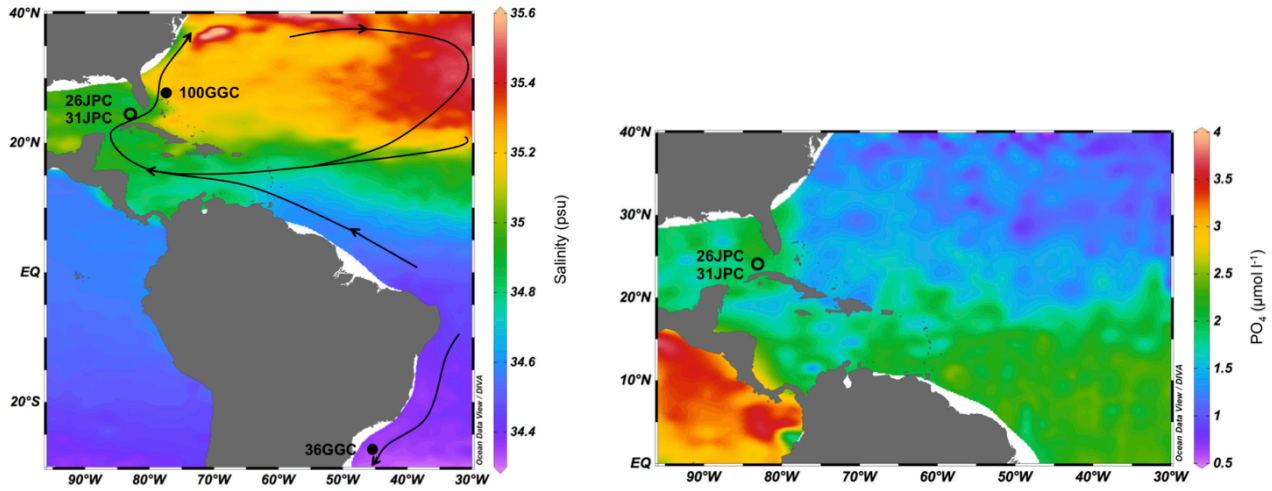

Figure 1-1 – Core locations. (left) Approximate location of Florida Straits cores KNR166-2-26JPC (24°19.61'N, 83°15.14'W, 546 m (this study)) and KNR166-2-31JPC (24°13'N, 83°18'W, 751 m (Came et al., 2008)) (open circle). Colors show salinity (psu) at potential density 27.3 kg m^{-3} (Garcia et al., 2014; Zweng et al., 2013), the isopycnal calculated for benthic waters at KNR166 2–26JPC. As waters circulate along constant density surfaces, salinity traces flow of different water masses through the straits as indicated by arrows. OCE205-2-100GGC (26°04'N, 78°02'W, 1057 m) and KNR159-5-36GGC (27°31'S, 46°28'W, 1268 m) (closed circles) measure northern subtropical gyre and South Atlantic waters, respectively (Came et al., 2008). (right) Modern PO4 (µmol L^{-1}) at potential density 27.3 kg m^{-3} (Garcia et al., 2014), with KNR166-2-26JPC and KNR166-2-31JPC approximate locations indicated (open circle).

1.2 Methods

We analyzed core KNR166-2-26JPC, recovered from 24°19.61'N, 83°15.14'W in the Florida Straits at 546 m water depth (Figure 1-1). The core is located on the landward side of the Florida current, where isopycnals are tilted to a shallower depth relative to the open North Atlantic due to the presence of Florida current. Today, this core location is situated in waters at potential density 27.3 kg m^3, an isopycnal that also characterizes Antarctic Intermediate Water.

Radiocarbon measurements on the planktonic foraminifera *Globigerinoides ruber* and *Globigerinoides sacculifer* were converted to calendar ages with the CALIB 7.1 calibration program and Marine13 marine reservoir calibration curve (Reimer et al., 2009) (Table 1-1). Calendar ages were then linearly interpolated for the depths between radiocarbon dates. Dates from between 344 and 408 cm were excluded from the age model as that interval of the core includes nonsequential ages and anomalously coarse sediments resembling laterally transported contourite deposits; see Lynch-Stieglitz et al. (2011). Sedimentation rates ranged from ~14 to 300 cm kyr^{-1}, with an average of ~70 cm kyr^{-1} from LGM to present.

Cd/Ca ratios were measured in tests of the aragonitic benthic foraminifer Hoeglundina elegans, excluding the 344–408 cm interval (~11.5–11.9 ka). Samples for analysis included 1–11 foraminifera tests each, picked from the >250 μm sieve fraction. Crushed tests were reductively and oxidatively cleaned using the methods of Boyle and Keigwin (1985) as modified by Boyle and Rosenthal (1996). Cd/Ca was measured using a Thermo Finnigan Element2 magnetic sector inductively coupled plasma–mass spectrometer following the methods delineated by Marchitto (2006). Analytical precision on Cd/Ca is ~ 2% (1σ) for samples >10 μg post- cleaning mass. Of 300 measurements, 13 were smaller than 1 μg after cleaning (based on Ca measurement) and are considered lost (not reported). One additional sample is omitted from plots due to high Al/Ca (>1,000 μmol mol^{-1}), and another is omitted because it is a Cd/Ca outlier, being >0.02 μmol mol^{-1} higher than both of its neighboring samples, suggesting contamination. Contamination indicators on the remaining samples were generally low: all but three Al/Ca <200 μmol

mol^{-1}, all Fe/Ca <100 μmol mol^{-1}, and all Mn/Ca <20 μmol mol^{-1}. Hoeglundina's aragonitic tests do not allow for manganese-calcium carbonate overgrowths that can alter trace metal content (Boyle et al., 1995).

Cd/Ca ratios were converted to seawater Cd concentration (Cd_W) using the relationship

$$D_p = \frac{\left(\frac{Cd}{Ca}\right) foram}{\left(\frac{Cd}{Ca}\right) water}$$

where the average partition coefficient D_p between the foraminifera and seawater in Hoeglundina is 1 for all water depths (Boyle et al., 1995). For the Cd_W calculation, the seawater Ca concentration is assumed to be the global mean value of 0.01 mol kg^{-1} (Boyle, 1992).

Table 1 – Radiocarbon Dates, KNR166-2 26JPC

Core depth	Species	^{14}C age	Error	Calendar age	Source
0.75	*G. Sacculifer*	1,070	70	640	Lynch-Stieglitz et al. (2011)
48.25	*G. Sacculifer*	2,990	30	2,760	Lynch-Stieglitz et al. (2011)
112.25	*G. Sacculifer*	6,720	40	7,250	Lynch-Stieglitz et al. (2011)
144.25	*G. Sacculifer*	8,100	80	8,570	Lynch-Stieglitz et al. (2011)
216.25	*G. Sacculifer*	9,550	40	10,416	Lynch-Stieglitz et al. (2011)
280.25	*G. Sacculifer and G. ruber*	10,100	45	11,110	Lynch-Stieglitz et al. (2011)

Core depth	Species	^{14}C age	Error	Calendar age	Source
344.25	*G. Sacculifer*	10,000	110	10,970	Lynch-Stieglitz et al. (2011)
356.25	*G. Sacculifer*	11,750	95	13,230[a]	Lynch-Stieglitz et al. (2011)
364.25	*G. Sacculifer and G. Ruber*	10,600	70	11,900[a]	Lynch-Stieglitz et al. (2011)
374.24	*G. Sacculifer*	10,500	50	11,688[a]	Lynch-Stieglitz et al. (2011)
392.25	*G. Ruber*	10,850	65	12,350[a]	Lynch-Stieglitz et al. (2011)
408.25	*G. Sacculifer and G. Ruber*	10,300	60	11,300[a]	Lynch-Stieglitz et al. (2011)
442.25	*G. Sacculifer and G. Ruber*	10,700	65	12,100	Lynch-Stieglitz et al. (2011)
464.25	*G. Sacculifer and G. Ruber*	10,800	55	12,280	Lynch-Stieglitz et al. (2011)
544.25	*G. Sacculifer and G. Ruber*	11,000	65	12,550	Lynch-Stieglitz et al. (2011)
592.25	*G. Ruber*	11,4000	65	12,860	Lynch-Stieglitz et al. (2011)
606.25	*G. Sacculifer*	11,600	35	13,090	Lynch-Stieglitz et al. (2011)
648.25	*G. Sacculifer*	12,350	200	13,830	Lynch-Stieglitz et al. (2011)
704.25	*G. Ruber*	13,500	55	15,710	This study
732.25	*G. Ruber*	15,000	60	17,780	Lynch-Stieglitz et al. (2011)
752.25	*G. Ruber*	15,550	70	18,410	This study
802.25	*G. Ruber*	17,750	80	20,920	Lynch-Stieglitz et al. (2011)
848.25	*G. Ruber*	20,300	120	23,940	Lynch-Stieglitz et al. (2014)
878.25	*G. Sacculifer and G.. Ruber*	21,300	95	25,230	Lynch-Stieglitz et al. (2011)
952.25	*G. Ruber*	26,300	130	30,140	Lynch-Stieglitz et al. (2011)
1014.25	*G. Ruber*	28,200	180	31,520	Lynch-Stieglitz et al. (2011)
1032.25	*G. Ruber*	28,200	590	31,830[a]	Lynch-Stieglitz et al. (2011)

Core depth	Species	^{14}C age	Error	Calendar age	Source
1074.25	*G. Ruber*	29,300	380	32,990	Lynch-Stieglitz et al. (2011)
1088.25	*G. Sacculifer and G. Ruber*	31,300	200	34,880a	Lynch-Stieglitz et al. (2014)
1104.25	*G. Sacculifer and G. Ruber*	30,600	170	34,220	Lynch-Stieglitz et al. (2014)
1118.25	*G. Sacculifer*	30,900	220	34,460	Lynch-Stieglitz et al. (2011)

Note. Calibrated using Calib 7.1 and Marine 13 curve. Calendar ages are rounded to nearest 10 years for radiocarbon ages with standard deviation >50 years, per Reimer et al. (2009). [a]Not used in age model.

1.3 Results

H. elegans Cd/Ca values range from 0.012 to 0.063 μmol mol^{-1} over the past 22 ka. The late Holocene (past 2 ka) Cd_W average is 0.37 nmol kg^{-1}, in good agreement with the phosphate-based prediction of 0.42 ± 0.10 nmol kg^{-1} for this core location (Bryan & Marchitto, 2010). Florida Straits seawater cadmium shows clearly lower values during the Last Glacial Maximum compared to the Holocene (Figure 1-2). A transition from lower LGM Cd_W levels to increased Cd_W occurs near 16 ka—about midway through the HS1. Cd_W reaches a maximum during the Bølling-Allerød North Atlantic warm period, near 14 ka. Cd_W then drops abruptly near the onset of the YD, remaining low before increasing to modern levels between 12 and 11.5 ka. The transition out of the YD appears to be abrupt, but this is obscured by the previously noted gap in the sediment record. Cd_W climbs slightly above modern levels during the early-middle Holocene (~9–6 ka) before declining toward the present.

1.4 Discussion

1.4.1 Florida Straits Seawater Cadmium and AMOC

The results presented in this study are consistent with a lower resolution Cd_w record generated from KNR166- 2-31JPC, located nearby in the Florida Straits at 24.22 N, 83.30 W, 751 m (Came et al., 2008). Cd_w variations in this record were interpreted to indicate AMOC strength, based on a comparison between the Florida Straits record and records from two other cores (Figure 1-2). Cd_w in a core from the Little Bahama Bank (26°04 N, 78°02 W, 1,057 m) reflects lower nutrient content in waters sourced in the North Atlantic and recirculated in the subtropical gyre. A core from the Brazil Margin (27°31 S, 46°28 W, 1,268 m) has higher Cd_w values representative of the higher-nutrient intermediate waters at the site. Recently, published Cd_w records from the Tobago Basin (11°36′N, 60°57′W, 852 m and 12°05′N, 61°14′W, 1,330 m) reinforce the view that AAIW Cd_w was higher than Cd_W in North Atlantic sourced waters throughout this time period (Poggemann et al., 2017). In the Florida Straits, lower Cd_w values imply a weaker AMOC, with reduced northward intrusion of high-nutrient waters from the south. The high nutrient levels of the southern sourced waters reflect the higher-nutrient Antarctic Intermediate Water (AAIW) and added nutrients from organic matter remineralization in the tropics. Higher Cd_w in the Florida Straits implies a greater presence of southern sourced water when overturning circulation, and North Atlantic Deep Water (NADW) production is strong. A section of phosphate measured in the region reveals greater nutrient gradient above 550 m (Roemmich & Wunsch, 1985), such that for a relaxation of

tilt of the isopycnals (expected when AMOC is reduced), a greater change in nutrient levels would be expected for the KNR166-2-26JPC site at 546 m than the KNR166-2-31JPC site at 751 m analyzed by Came et al. (2008). This is consistent with the lower Cd_w values in the KNR166-2-26JPC record relative to that of KNR166-2-31JPC during the YD, even as both sites record lower nutrients in that period relative to the Bølling-Allerød, indicating reduced AMOC surface return flow.

The Brazilian Margin record cannot be considered a true end-member for determining the relative northern and southern water contributions at the Florida Straits. The waters entering the Caribbean from the south on this density surface have higher salinity relative to the Brazil Margin site (Figure 1-1, left), implying significant dilution of AAIW. On the other hand, the nutrient values of waters entering the Caribbean from the south are similar to those at the Brazil Margin, as the dilution of AAIW by lower-nutrient northern sourced waters is compensated by the ingrowth of nutrients by the remineralization of organic matter (Figure 1-1, right). Despite these complications, we expect that in the past, the nutrient content of waters entering the Caribbean from the tropics was higher relative to that of North Atlantic gyre water, as it is today. We will thus interpret high Cd_w in the Florida Straits as reflecting a strong inflow of water from the south as in (Came et al., 2008).

For both the KNR166-2-26JPC and KNR166-2-31JPC records, Florida Straits intermediate waters appeared dominated by northern sources during the LGM and YD and by southern influxes during the Bølling-Allerød and Holocene (Figure 1-2). The

KNR166-2-26JPC record also shows lower Cd_w during only the first half of HS1, suggesting AMOC strengthened midway through that interval.

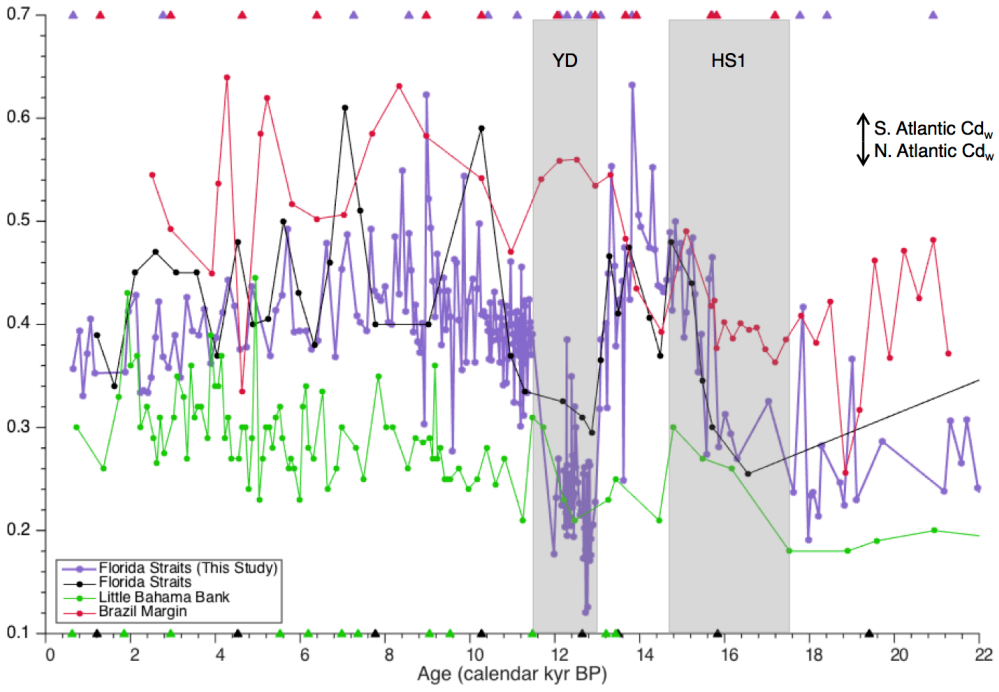

Figure 1-2 – Benthic Cd_W of the Atlantic cores versus age. Violet: Florida Straits, this study, 546 m depth. Red: Brazil Margin 1,268 m. Black: Florida Straits, 751 m. Green: Little Bahama Bank, 1,057 m, all from Came et al. (2008). Radiocarbon age control dates of the cores are indicated with triangles of corresponding colors. Gray bars indicate boundaries of the Younger Dryas and Heinrich Stadial 1.

1.4.2 Co-located Proxy Comparisons

A Florida Straits neodymium isotope record indicates similar timing of local water mass changes as interpreted from the high-resolution Cd_w record. Nd isotope ratios trace water masses independently of biological processes. Today, the ratio for the water masses sourced in the North Atlantic is near $\varepsilon_{Nd} = 13.5$ (Piepgras & Wasserburg, 1980, 1987) and

higher, 6 to 9, for waters sourced in the Southern Ocean (Jeandel, 1993). The difference is due to the input of older weathered continental material (low ε_{Nd}) into the Atlantic and newer volcanic weathered material (high ε_{Nd}) in the Pacific, a mixture of which contributes to the Southern Ocean water ε_{Nd} ratio. Comparing the KNR166-2-26 JPC Cd_w record with ε_{Nd} from the same core (Xie et al., 2012), the timing of transitions into and out of the deglacial cold periods is in overall agreement (Figure 1-3c). As with the Cd_w record, authigenic ε_{Nd} transitions from more northern like to more southern like values between ~16 ka into the Bølling-Allerød and declines again into more northern values at the start of the YD. This suggests that AMOC weakened such that AAIW intrusion declined during early HS1 and the YD and that AMOC recovered during late HS1 and the Bølling-Allerød.

A record of benthic foraminifera $\delta^{18}O$ in the Florida Straits is interpreted to reflect changes in AMOC strength, which change the density gradient across the Straits, and also suggests weakened AMOC associated with meltwater events (Lynch-Stieglitz et al., 2011, 2014). The density gradient increases with increased vertical shear in the Gulf Stream as it travels through the Florida Straits. When flow weakens, isopycnal tilt between the Florida side and the Bahamas side of the Straits flattens (Lynch-Stieglitz et al., 1999). For KNR166-2-26JPC on the Florida side, this is apparent as a decrease in $\delta^{18}O$ (reduced density) during mid-HS1 and the YD. That the $\delta^{18}O$ transitions are concurrent with those of Cd_w (Figure 1-3a) provides further validation for the link between AMOC strength and local water mass changes. Flattening of isopycnals places the core depth in lower-nutrient water as density surfaces that were shallower in a

stronger AMOC regime reach the 546 m depth of the core location when AMOC is weaker. However, Florida Straits nutrient changes cannot be explained entirely by this effect. By comparing modern phosphate (Roemmich & Wunsch, 1985) and inferred isopycnal tilt based on Younger Dryas oxygen isotope data from the Florida Straits (Lynch-Stieglitz et al., 2011), we find that isopycnal tilt flattening can explain some, but not all, changes in Cd_w during the Younger Dryas.

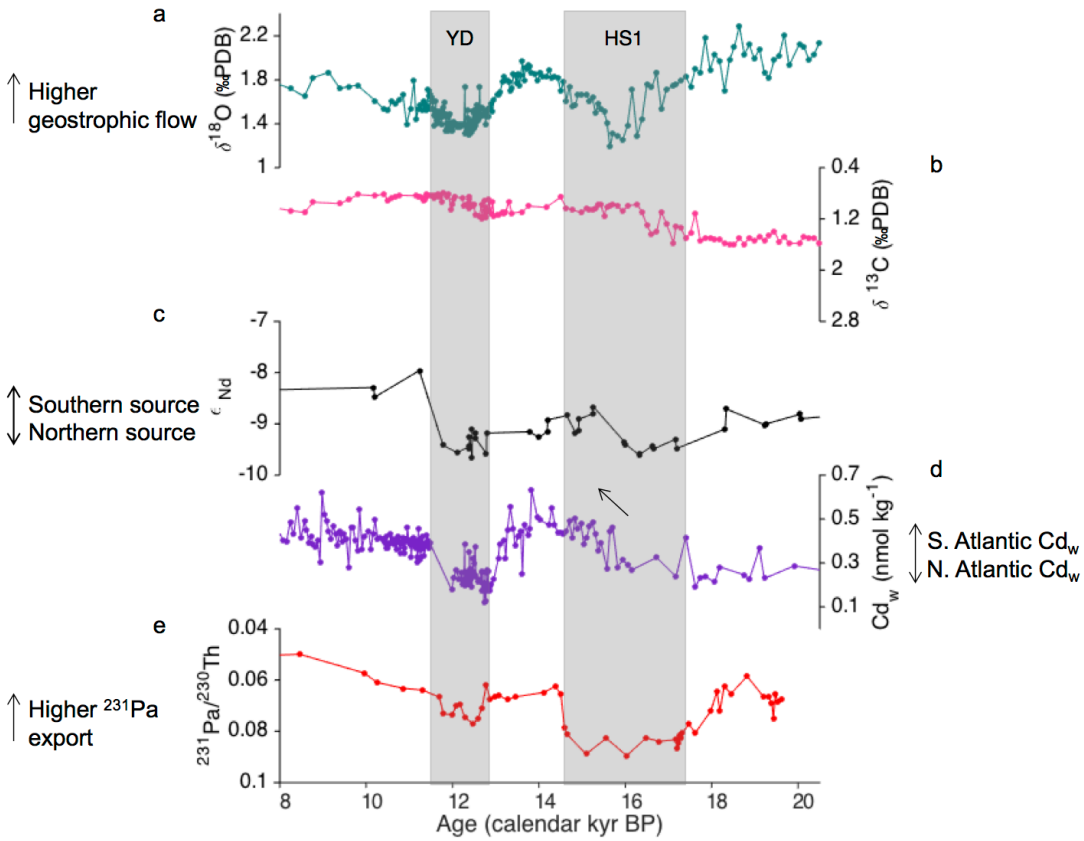

Figure 1-3 – Tracers of North Atlantic circulation over deglaciation. From Florida Straits (KNR166-2-26JPC): (a) Ice volume- corrected benthic $\delta^{18}O$ (Lynch-Stieglitz et al., 2014). (b) Benthic $\delta^{13}C$ (Lynch-Stieglitz et al., 2014) scaled to phosphate per (Broecker & Maier Reimer, 1992). (c) Authigenic ε_{Nd} (Xie et al., 2012). (d) Benthic

Cd_w (this study). (e) $^{231}Pa/^{230}Th$ from the Bermuda Rise (McManus et al., 2004). All proxies are plotted so that arrows up indicate stronger AMOC.

These co-located proxy records bolster our conclusion that AMOC strength determines the proportions of water masses that dominate the Florida Straits, and that those water mass changes control Cd_w changes in the region. In contrast, a model study (Schmittner & Lund, 2015) shows that carbon from respired organic matter in the upper North Atlantic accumulates during periods of weakened AMOC, which would eventually counteract the reduced import of high-nutrient southern source waters. While Cd_w in the Florida Straits does rise somewhat gradually over HS1, contemporary changes in same-core ε_{Nd} and $\delta^{18}O$, which are not nutrient proxies, support interpreting the rising Cd_w as an increase of southern sourced water transport and not a localized accumulation of remineralized nutrients.

In the Florida Straits, changes in $\delta^{13}C$ do not directly reflect AMOC variability: changes in $\delta^{13}C$ over deglaciation do not correlate with water mass changes as indicated by Cd_w and ε_{Nd} in the core record (Figure 1-3). While Cd_w reflects large changes in nutrient levels, the $\delta^{13}C$ signal is more muted when placed on an equivalent scale. The distinction between high $\delta^{13}C$ in lower-nutrient northern sourced waters and low $\delta^{13}C$ in higher-nutrient southern sourced waters is dampened by opposing effects of air-sea exchange on the carbon isotope fractionation at the sites of water mass formation (Lynch-Stieglitz & Fairbanks, 1994).

1.4.3 *Comparison with Other Atlantic Records*

The McManus et al., 2004 study employed the $^{231}Pa/^{230}Th$ circulation tracer at the Bermuda Rise to show evidence of AMOC decline during HS1 and the YD. While the transitions into and out of the YD cold period are similarly timed in $^{231}Pa/^{230}Th$ and the Florida Straits Cd_w record, the period of high $^{231}Pa/^{230}Th$ during HS1 spans 17.5–14.7 ka. In that record, AMOC recovery at the end of HS1 appears to occur rapidly, over about 200 years from 14.7 to 14.5 ka (Figure 1-3e). By contrast, the Florida Straits Cd_w record implies a more gradual recovery beginning near 15.7 ka (Figure 1-3d).

Given the distance between the two core sites, it is logical to question whether any local effects on the radiocarbon dates used to establish the age models applied to the records could explain the difference in timing and rate of AMOC changes out of HS1. Both KNR166-2-26JPC, from the Florida Straits, and OCE326-GGC5, from the Bermuda rise, are located in regions with well-equilibrated surface waters. Surface waters with the oldest apparent radiocarbon ages are found in upwelling zones, where older, ^{14}C depleted waters are brought to the surface. Butzin, Prange, and Lohmann (2012) and Franke, Paul, and Schulz (2008) employed model simulations of ocean ^{14}C with variable climate conditions over the deglaciation. In these studies, ventilation changes between the LGM and modern oceans do imply large radiocarbon age differences between the periods in

some regions. Yet for our sites of comparison, no offsets between the two locations are indicated. For these reasons, we reject reservoir age as an explanation for the discrepancy.

It is plausible that the upper branch of AMOC, as recorded by multiple tracers in the Florida Straits, strengthens near 16 ka, while changes in the abyssal Atlantic occurred later. Bradtmiller, McManus, and Robinson (2014) synthesize data from multiple cores at various depths across the Atlantic. These $^{231}Pa/^{230}Th$ records show that AMOC was likely diminished but not entirely shut off during HS1 and LGM. Their interpretation indicates greater transport in intermediate waters than in deep waters during those periods, unlike the Holocene, when the North Atlantic is well ventilated at all depths. It is therefore possible that the Florida Straits Cd_W recorded an earlier strengthening of the shallower cell during mid-HS1, whereas $^{231}Pa/^{230}Th$ from 4.55 km depth on Bermuda rise captured a later reinvigoration of deep AMOC, indicating enhanced NADW production.

Data from other Atlantic records could support this interpretation. Huang, Oppo, and Curry (2014) found that their three ε_{Nd} records from intermediate depths near Demerara Rise off the Brazilian coast show a two-phase AMOC strength trend within HS1. In the first phase, ~18–16 ka, ε_{Nd} values indicate a reduced AAIW component of the local water mass; in the second phase, ~15.5–14.7 ka, the AAIW fraction has increased, which is interpreted as a partial AMOC recovery. Near the South Iceland Rise, an abrupt, localized decrease in the ^{14}C age of waters ~1–2 km depth at 16 ka has been attributed to enhanced ventilation via rerouting of freshwater overflow from the northwest to the northeast Atlantic, enhancing sea ice and brine production (Thornalley et al., 2011). This

change contrasts with the NGRIP ice core $\delta^{18}O$ record showing polar warming not evident until the start of the Bølling-Allerød (Andersen et al., 2004; Rasmussen et al., 2006). These findings also suggest a decoupling of shallow overturning, which may have strengthened earlier coming out of HS1, from deeper circulation which may have lagged. However, even if full overturning did not restart until the start of the Bølling-Allerød, it is important to note that changes in shallow overturning could also force atmospheric change.

The interpretation of low Cd_w values as weakened AMOC during the late last glacial period (~18–20 ka) is difficult to reconcile with other records of deglacial circulation (e.g., Gherardi et al., 2009; Huang et al., 2014; McManus et al., 2004), which imply stronger AMOC during the late glacial period relative to the early HS1. It is possible that at this location, nutrient changes associated with the weakening of upper AMOC return flow at the start of HS1 are not distinguishable in an already stratified glacial North Atlantic. As the nutrient structure and overturning regime of the Atlantic at LGM remains uncertain, it is unclear whether extending this type of Cd_w analysis through the glacial is appropriate at this site. Because of these complications, we decline to interpret the lack of significant change in Cd_w the late glacial to early HS1 period in terms of circulation.

1.4.4 *Climate Implications of a Mid-Heinrich Stadial 1 AMOC Recovery*

The increase of Cd_w in the Florida Straits record near 16 ka implies a mid-HS1 AMOC recovery. If AMOC resumed before the end of HS1, it should also be apparent in climate records. An obvious indication of the resumption of upper AMOC and its

associated northward heat transport would be a temperature increase in North Atlantic surface waters. Indeed, this is indicated near 16 ka in several sea surface temperature proxy records from the subpolar North Atlantic (Bond et al., 1993; Hodell et al., 2017; Naafs et al., 2013).

Increased AMOC leads to warming in the Northern Hemisphere (and potentially cooling in the Southern Hemisphere), which fuels Northern Hemisphere monsoon systems (Parsons et al., 2014). Furthermore, increases in AMOC northward heat transport have been linked to northward shifts of the Intertropical Convergence Zone (ITCZ) (Cheng et al., 2012; Chiang et al., 2003; Deplazes et al., 2013). An abrupt weakening of the East Asian Summer Monsoon (EASM), thought to correlate with maximum southern ITCZ displacement at 16.1 ka, is inferred from Chinese speleothem records (Wang et al., 2001; Zhang et al., 2014). The Hulu Cave record shows evidence of EASM weakening during six Heinrich Stadials, which Zhang et al. (2014) link to AMOC variability and southern ITCZ displacement. If EASM strength is tied to AMOC, as AMOC weakens, so should EASM (indicated by higher $\delta^{18}O$, interpreted as lower summer precipitation), via atmospheric and oceanic teleconnections. Hulu and Qingtan Cave records are consistent with AMOC changes over the middle-to-late HS1, as evident in the Florida Straits Cd_W record. The trend of reduced to gradually increasing precipitation coincides with upper branch AMOC recovery during the later HS1, as expected.

A record from the San Làzaro Basin on the California Margin shows that the YD and HS1 are locally marked by high surface water $\delta^{18}O$ (Rodríguez Sanz et al., 2013). Saltier conditions observed in those periods are ascribed to a weakening California current,

which prevented the advection of colder fresher water as observed in the Holocene. The authors link the weakening current to the southward shift of the ITCZ and the North Pacific High. Also observed is a distinct two-phase structure to the local expression of HS1. A sharp transition from saltier to fresher conditions in the San Làzaro Basin starting at 16.2 ± 0.8 ka is consistent with the timing and trends of ITCZ maximum southern displacement recorded in the Chinese speleothems and with the mid-HS1 recovery of AMOC recorded in the Florida Straits.

Questions remain regarding the timing of ice rafting events within the Heinrich Stadial period (Hemming, 2004). This uncertainty further complicates understanding the sequence between ice sheet collapse, AMOC change, and climate variability (Marshall & Koutnik, 2006), and it reinforces the question of why weakened AMOC persisted throughout HS1 at depth as indicated by Gherardi et al. (2009), Hall et al. (2011), and McManus et al. (2004) and other records. Nevertheless, the Florida Straits Cd_w record supports evidence of a recovery of AMOC strength beginning near 15.7 ka and before the HS1 period terminates, as expressed in ice core $\delta^{18}O$ (Andersen et al., 2004), North Atlantic $^{231}Pa/^{230}Th$ (McManus et al., 2004), and other records.

1.5 Conclusions

The new benthic seawater cadmium record provides a high-resolution record of circulation changes over the last deglaciation in the Florida Straits. Multiple proxy records from the same core support the interpretation of periods of diminished Cd_w during Heinrich Stadial 1 and the Younger Dryas as indicative of reduced overturning

circulation in the North Atlantic. The record builds on existing evidence of a resumption of AMOC strength near 16 ka, which is coherent with evidence for mid-HS1 ITCZ migration. Further investigation into the timing and locations of deglacial freshwater input, AMOC variability, and related climate impacts is warranted. To that end, this Cd_w record provides compelling evidence from the upper ocean for a mid-HS1 AMOC recovery against which other proxy measurements over HS1 can be compared.

1.6 Acknowledgements

We thank Jerry McManus and the reviewers for helpful discussion and Tiee-Yuh Chang and Brigitta Rongstad for laboratory assistance. This work was funded by the NSF Graduate Research Fellowship DGE-1148903 (S.V.) and NSF grant OCE-1459563 (J.L.S.). Data are archived in the NOAA National Centers for Environmental Information database (https://www.ncdc.noaa.gov/paleo- search/study/22314).

CHAPTER 2. INTERMEDIATE WATER CIRCULATION CHANGES IN THE FLORIDA STRAITS FROM A 35 KA RECORD OF MG/LI-DERIVED TEMPERATURE AND CD/CA-DERIVED SEAWATER CADMIUM

(Previously published as: Valley, Shannon G., Lynch-Stieglitz, J., and Marchitto, Thomas M., 2019. Intermediate water circulation changes in the Florida Straits from a 35 ka record of Mg/Li-derived temperature and Cd/Ca-derived seawater cadmium. Earth Planet. Sc. Lett. 523, 115692.)

2.1 Introduction

Changes in Atlantic Meridional Overturning Circulation (AMOC) contribute to reorganizing the global distribution of heat and precipitation, and so contribute to long-term and abrupt climate change over glacial and interglacial periods. During the Last Glacial Maximum (LGM), North Atlantic Deepwater production was likely reduced, resulting in a shoaled water mass in the North Atlantic, the characteristics of which are only broadly understood (Lynch-Stieglitz, 2017). Today, intermediate-depth waters in the Florida Straits make up part of the upper branch of AMOC. Numerous studies have reconstructed intermediate water properties in the western tropical Atlantic and interpreted them in terms of environmental changes locally and/or in the source region over glacial-interglacial intervals (e.g. Huang et al., 2014; Poggemann et al., 2018) but only a few (e.g. Came et al., 2007; Schmidt et al., 2012; Weldeab et al., 2016) have included temperature reconstructions that also enable estimates of seawater $\delta^{18}O$. Changes in seawater $\delta^{18}O$ in the subsurface ocean can indicate changes in land ice volume as well as hydrological changes at the water mass source region.

Well-constrained estimates of paleo-temperatures in deeper waters have likewise been limited. Mg/Ca measured in plank- tonic foraminifera has been extensively applied to reconstruct sea surface and near subsurface temperatures but use in benthic foraminifera has been hampered by confounding factors. The carbonate ion saturation state of seawater affects Mg incorporation in benthic foraminifera, particularly at temperatures below 3°C (Yu and Elderfield, 2008). Mg/Ca-derived temperature estimates are also complicated by the influence of salinity on Mg uptake in planktonic foraminifera (Honisch et al., 2013) and inter-species calibration variability. Mg/Ca-derived temperature reconstructions in benthic foraminifera have standard error temperature equivalents ranging between 1.0-4.5°C (Bryan and Marchitto, 2008; Lea, 2014, and references therein).

Instead, the application of the Li/Ca to Mg/Ca ratio (Li/Mg, or Mg/Li) has been empirically demonstrated to improve upon Mg/Ca or Li/Ca temperature calibrations from tropical and cold water corals, as well as from the aragonitic benthic foraminifer *Hoeglundina elegans* (Case et al., 2010; Raddatz et al., 2013; Montagna et al., 2014; Bryan and Marchitto, 2008). It has been postulated that Li/Mg improves upon Mg/Ca measurements by normalizing for vital effects associated with the adjustment of metal ions from seawater imported into the organism's calcification space (Case et al., 2010; Bryan and Marchitto, 2008; Marchitto et al., 2018). Strikingly similar temperature calibration curves for both *H. elegans* and across numerous coral taxa (Marchitto et al., 2018) suggest that the Li/Mg ratios in these organisms are more strictly temperature dependent than Li/Ca or Mg/Ca ratios. The standard error of about ±1.0°C for the coldest seawater temperatures derived from Li/Mg (and its inverse, Mg/Li) represents significant

improvement to intermediate and bottom water temperature re- construction. In this study, we apply the Mg/Li temperature proxy in benthic foraminifera in order to characterize intermediate water in the Florida Straits, presenting temperature and derived seawater $\delta^{18}O$ through the Marine Isotope Stage (MIS) 2/3 boundary.

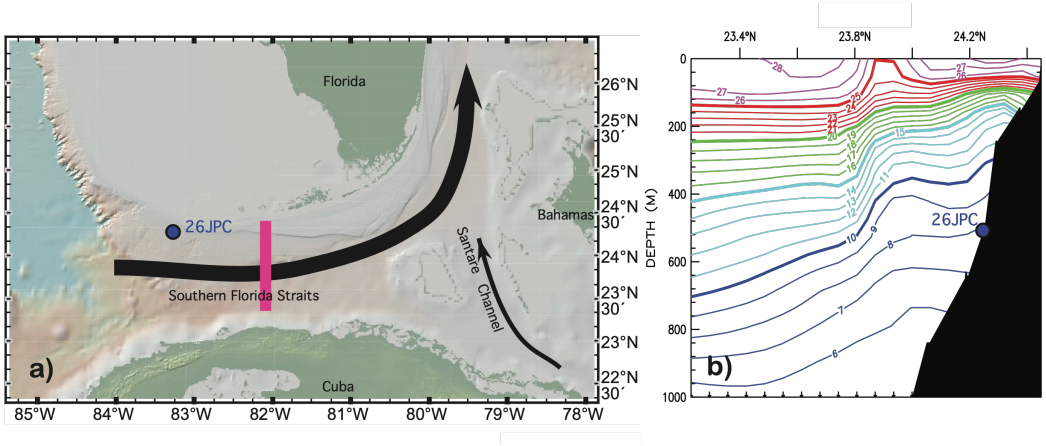

Figure 2-1 – Location of core KNR166-2 26JPC (24°19.61′N, 83°15.14′W, 546 m, blue point), recovered from the Florida Straits. a) The large black arrow indicates the direction of the Florida Current which contains upper AMOC return flow through the Florida Straits. b) Core location is indicated in a meridional the cross section of temperature in °C (Marchitto et al., 2007) at 82°W (pink in Fig. 2-1a).

Surfaces of constant temperature and density are steeply tilted upward toward the Florida margin at our core location reflecting the largely geostrophic flow of the Florida Current (Fig. 2-1). Today, this is evident in a cross-basin temperature gradient of ~4 ° C (Roemmich and Wunsch, 1985). Lynch-Stieglitz et al. (1999) inferred a reduction of AMOC during periods associated with North Atlantic freshwater influx during the last deglaciation from the reduction of the cross-basin density gradient, as estimated from the $\delta^{18}O$ of benthic foraminifera. Using the same sediment core that we analyze in this study,

these authors proposed that the gradient reductions and benthic $\delta^{18}O$ minima during Heinrich Stadial 1 (HS1) and the Younger Dryas (YD) were associated with warming in Florida Straits intermediate waters. Our new Mg/Li-temperature data enable us to verify that the $\delta^{18}O$ minima excursions are indeed representing warming, due in part to the flattening of the isopycnals across the Florida Straits, rather than freshening.

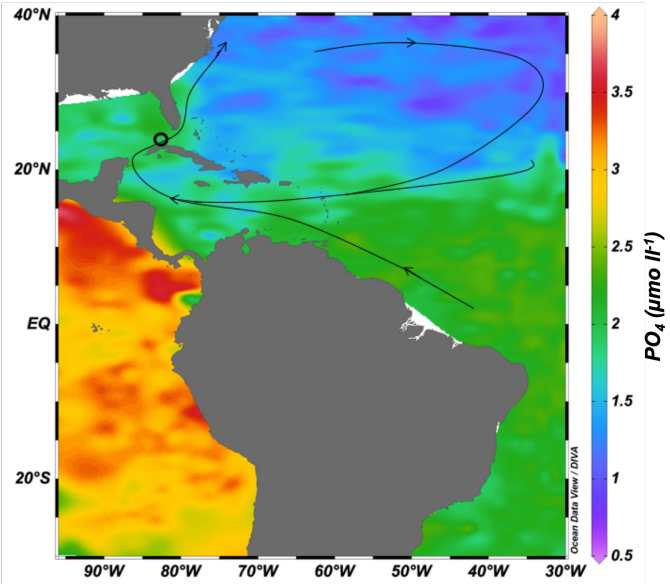

Figure 2-2 – Core location (open circle) and large-scale upper ocean circulation patterns (black arrows). Colors indicate phosphate at potential density 27.3 kg m^{-3} (Garcia et al., 2014), the density at the KNR166-2 26JPC core site.

Seawater cadmium (Cd_w) has a profile similar to phosphate in the modern ocean (Boyle et al., 1976) and can be applied as nutrient proxy to trace circulation change (Fig. 2-2). In a previous work, we reconstructed Cd_w over the deglaciation (~0-25 ka) in the Florida Straits (Valley et al., 2017), again using the same sediment core that we analyze in this study. Using the framework presented in (Came et al., 2008), which interpreted

high Cd_w values in terms of a strong overturning circulation, we found support for weak AMOC during early Heinrich Stadial 1, with upper AMOC resuming strength midway through the Heinrich Stadial. Also in agreement with Lynch-Stieglitz et al. (2014), we found evidence for an AMOC reduction during the YD.

Lynch-Stieglitz et al. (2014) in their study based on the oxygen isotope values of benthic foraminifera did not find evidence for AMOC changes over Heinrich Stadials 2 and 3, while Them et al. (2015) present evidence for AMOC changes over some of the Dansgaard-Oeschger (D-O) events. Here we extend our reconstruction of seawater cadmium to AMOC through ~35 ka, which will give us additional evidence to support these inferences about AMOC variability during MIS 2 and 3.

2.2 Methods

Samples were analyzed from the sediment core, KNR166-2 26JPC, retrieved from the Florida Straits in the western central Atlantic (24° 19.61'N, 83° 15.14'W, 546 m depth). Sedimentation rates in this core ranged between ~14-300 cm kyr^{-1} , with an average ~70 cm kyr^{-1} dated from the LGM to modern. The age model was previously published in Valley et al. (2017).

Mg/Ca, Li/Ca, and Cd/Ca ratios were measured in the tests of the benthic foraminifer *Hoeglundina elegans*, following the reductive and oxidative cleaning procedures of Boyle and Keigwin (1985) as modified by Boyle and Rosenthal (1996). One to 11 >250 μm individual foraminifera per sample were analyzed for trace and minor element ratios on a Thermo Finnigan Element2 magnetic sector inductively coupled plasma-mass

spectrometer using the methods of Marchitto (2006). Analytical precision (1σ) is 0.5% for Mg/Ca, 0.9% for Li/Ca, and 2% for Cd/Ca. Of the 426 samples analyzed, 28 were discarded due to small post-cleaning size (< 5 μg) and 9 due to high concentrations of contaminant metals (> 100 of either Al, Fe, Mn μmol mol^{-1}) (Bryan and Marchitto, 2008).

Temperatures were derived from Mg/Li ratios using the empirically derived polynomial calibration equation for *H. elegans*:

$$Mg/Li = 0.150 \pm 0.012 + 0.0209 \pm 0.0027T - 0.0002 \pm 0.0001\ T^2$$

(Marchitto et al., 2018). We apply this polynomial equation using the Mg to Li ratio, rather than exponential equations derived using either Mg/Li or Li/Mg, because it has been demonstrated to provide more accurate temperatures in *H. elegans* (for comparison, Li/Mg-derived temperatures are included in supplementary materials). The fit of this equation corresponds to $r^2 = 0.95$, and the standard error (1σ) for Mg/Li is 0.022 mol $mmol^{-1}$, equivalent to ±1.0°C at 0°C and ±1.7°C at 20°C.

By using Mg/Li-derived temperature as an independent means to reconstruct temperature, we are able to constrain changes in $\delta^{18}O$ of seawater ($\delta^{18}O_w$) in our record. $\delta^{18}O_w$ is calculated by

$$(\delta^{18}O_c - \delta^{18}O_w + 0.27) = -0.245 \pm 0.005\ t + 0.0011 \pm 0.0002\ t^2 + 3.58 \pm 0.02$$

where t is temperature in Celsius, $\delta^{18}O_c$ is $\delta^{18}O$ of $CaCO_3$ from benthic foraminifera scaled in PDB (PeeDee Belemnite), and $\delta^{18}O_w$ is scaled in SMOW (Standard Mean

Ocean Water) (Marchitto et al., 2014). The propagated uncertainty for derived $\delta^{18}O_w$ is 0.32‰. The oxygen isotope values have been corrected for the expected whole ocean change due to the melting of the continental ice sheets using the sea level data by Siddall et al. (2009), assuming a 120 glacial sea level drop corresponds to a 1.05‰ increase in $\delta^{18}O_W$ (Schrag et al., 2002).

Cd_w was calculated from Cd/Ca using a depth independent partition coefficient of 1 for *H. elegans* (Boyle et al., 1995) and assumed global mean seawater Ca concentration 0.01 mol kg^{-1} (Boyle, 1992). In order to identify outliers, the paleotemperature and Cd_W data were smoothed using the function smooth.m (Matlab version R2017b) with a robust Lowess smoothing method and 1% data smoothing window. Outliers beyond 2σ of the smoothed time series were omitted (4% of temperature and 5% Cd_W data). The remaining data points are retained in our plots and interpretation. All data are in a supplementary table, with the omitted points marked.

2.3 Results

Temperatures in the late Holocene, 6,000-600 yr before present, averaged 6.8 ± 1.2˚C (including standard error), near to the observed bottom water temperature of 7.0°C (Marchitto et al., 2007; Fig. 2-3a). Reconstructed intermediate water temperature reveals a glacial-Holocene difference of 3.2°C. This difference seems reasonable given the 2.4 ± 2.2°C change estimated for Atlantic sea surface temperature (SST) (Waelbroeck et al., 2009). Temperatures rise from the glacial to near-modern values between 18.2 and 16 ka.

An additional transient warming of about 2.0°C occurred in the record during the YD, relative to mean temperatures in the pre- ceding Bølling-Allerød and following Holocene periods. From the Bølling-Allerød to the present, the temperature record closely resembles the ice volume-corrected δ^{18}O-calcite record (Fig. 2-3c) in both pattern and magnitude of inferred temperature change. In the first 500 yr of the record, during Late MIS3, Mg/Li temperatures were less than 1°C cooler than in the Holocene.

A record of seawater cadmium, extended beyond the ~20 kyr previously published in Valley et al., 2017, shows glacial Cd_w is on average 0.12 μmol mol^{-1} lower than during the Holocene. This lower average is punctuated by abrupt peaks in Cd_w, including a particularly large peak approximately 0.15 μmol mol^{-1} above sur- rounding values centered near 28 ka. Cd_w during the late MIS 3 was more variable but averaged near glacial values.

2.4 Discussion

2.4.1 LGM water mass properties

Cd/Ca measured in benthic foraminifera has been used to reconstruct seawater cadmium (Cd_w), which has a profile similar to the nutrient phosphate in the ocean (Boyle et al., 1976). This technique of applying Cd_w as a nutrient tracer of water masses has been used to infer changes in AMOC in the Florida Straits (Came et al., 2008; Valley et al., 2017). The densest waters in the Florida Straits are part of the upper branch of AMOC and have high nutrient concentrations reflecting their origin in the Southern Hemisphere and the addition of nutrients in the tropics (Palter and Lozier, 2008) (Fig. 2-2). During the

LGM we observe that Cd_w levels were generally low, with a glacial-interglacial difference of about −0.2 nmol kg^{-1} (Figs. 2-3, 2-4). This glacial trend is consistent with other nutrient reconstructions of the upper interior North Atlantic (Marchitto and Broecker, 2006; Zahn and Stuber, 2002; Oppo et al., 2018) that identify lower nutrient waters at these depths as characteristic of Glacial North Atlantic Intermediate Water (GNAIW). Low nutrient values could be associated with lower preformed nutrients in GNAIW as compared to Antarctic Intermediate Water (AAIW), or with lower remineralization.

The glacial-Holocene difference in $\delta^{18}O_c$ at our location is 1.31‰, or 0.27‰ when corrected for changes in global ice volume (Schrag et al., 2002). The derived glacial-interglacial change in $\delta^{18}O_w$ from the Florida Straits is 0.57‰ (−0.49‰ ice-volume corrected), which is lower than the estimated 0.7-0.8‰ (uncorrected) average for Atlantic waters below 1000 m (Schrag et al., 1996; Adkins and Schrag, 2001; Schrag et al., 2002), and also lower than another tropical Atlantic site at intermediate depth (~ 1‰, uncorrected, at 1295 m, Weldeab et al., 2016).

The Mg/Li temperature, $\delta^{18}O_w$ and Cd_w records suggest cold, relatively fresh and low-nutrient waters in the Florida Straits during the LGM. These properties do not match either the AAIW in this region today (cold, fresh, high-nutrient) or intermediate waters formed in the North Atlantic (warmer, saltier, low-nutrient). This implies significant change in the locations or mechanisms of intermediate water formation during the height of the last ice age. Additional proxy data for intermediate water properties at other locations, as well as surface water properties near to the sites of intermediate water

formation are needed to develop well founded hypotheses about the origin of this cold and fresh water.

2.4.2 Glacial-aged Heinrich events

The lack of substantial warming in the KNR-166-2 26JPC Mg/Li subsurface temperature record during HS2 and HS3 (Fig. 2-4) is consistent with the lack of Caribbean subsurface warming for those periods (Parker et al., 2015) and supports the idea that at these times AMOC was not greatly reduced (Lynch-Stieglitz et al., 2014).

The absence of a weakened-AMOC signal during HS2 and 3 in the temperature record is paralleled by a lack of a coherent Cd_w nutrient signal in those periods. HS3 has been associated with lower quantities of ice rafted debris relative to other Heinrich events (McManus et al., 1998). Moreover, it is possible that as AMOC was already reduced during peak glaciation, the high latitude influx of freshwater associated with Heinrich events 2 and 3 did not weaken AMOC any further.

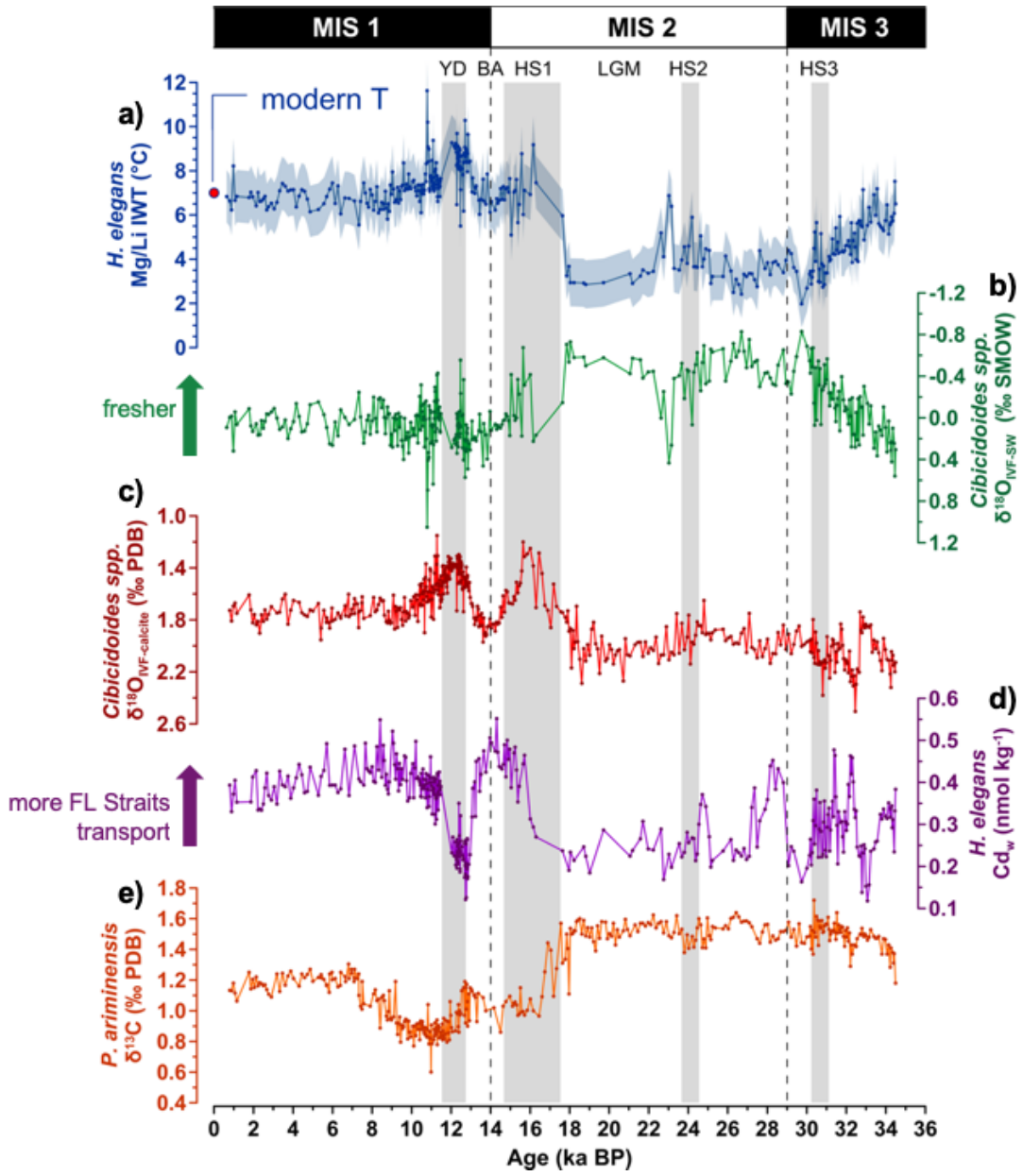

Figure 2-3 – Proxies measured in benthic foraminifera in core KNR166-2 26JPC. The Younger Dryas and Heinrich Stadials are shaded in gray. a) Mg/Li-derived intermediate water temperature, this study, with error range (1σ) and modern observed temperature indicated (Marchitto et al., 2007), b) calculated $\delta^{18}O$ of seawater, ice-volume corrected assuming a 1.05‰ increase in $\delta^{18}O_{SW}$ and 120 m sea level reduction during LGM (Schrag et al., 2002; Siddall et al., 2009), c) $\delta^{18}O$ of benthic foraminifera, ice-volume corrected, Lynch-Stieglitz et al., 2014. Axis is scaled to temperature, d) Cd_w, Valley et al., 2017 and this study, e) $\delta^{13}C$, Lynch-Stieglitz et al., 2014. Age model is based on ^{14}C dating per Valley et al., 2017.

2.4.3 AMOC variability over deglaciation

In our previous work we found evidence for decreased AMOC during the YD and early HS1 based on both the $\delta^{18}O$ in benthic foraminifera (Lynch-Stieglitz et al., 2011; Lynch-Stieglitz et al., 2014) and Cd_w reconstructions in the Florida Straits (Valley et al., 2017). The interpretation of the oxygen isotope data is supported by the new temperature record. If reduced AMOC caused a relaxation of the tilted isotherms across the Straits at this water depth, this alone could account for the 2°C warming observed in our Mg/Li subsurface temperature record during the YD, as shown by an ocean modeling study (Lynch-Stieglitz, 2014). Warming is also evident during Heinrich Stadial 1 (HS1), by about 2.5°C above late LGM levels near 17 ka. It is difficult to establish how much of temperature change throughout HS1 is due to changes in AMOC vs. regional deglacial warming due to other causes without a similarly resolved temperature time series on the other side of the Florida Straits. However, average temperatures during the latter half of HS1 are not higher than during the Holocene and Bølling-Allerød. This is consistent with evidence of upper-branch AMOC resumption based on the rise in Cd_w beginning near 16 ka (Huang et al., 2014; Valley et al., 2017).

Beyond the effect of density surface adjustment in the Florida Straits, other mechanisms for warming in subsurface to intermediate-depth waters in the subtropical and tropical Atlantic have been proposed. AMOC reduction in response to high-latitude fresh- water input has been linked to intermediate depth warming of ~2-6°C in models and paleo-data interpretations. Such warming has been proposed to result from reduced ventilation by colder waters from the south (Rühlemann et al., 2004; Came et al., 2007),

increased advection of warmer North Atlantic subtropical gyre water (Schmidt et al., 2012), enhanced downward heat diffusion (Weldeab et al., 2016), and warming of intermediate waters at their southern ocean formation site (Poggemann et al., 2018). Regardless of the mechanism(s) causing abrupt Florida Straits intermediate water warming during the last deglaciation, this Mg/Li- derived temperature record reinforces existing evidence for a generalized tropical Atlantic subsurface warming response to AMOC slowdown.

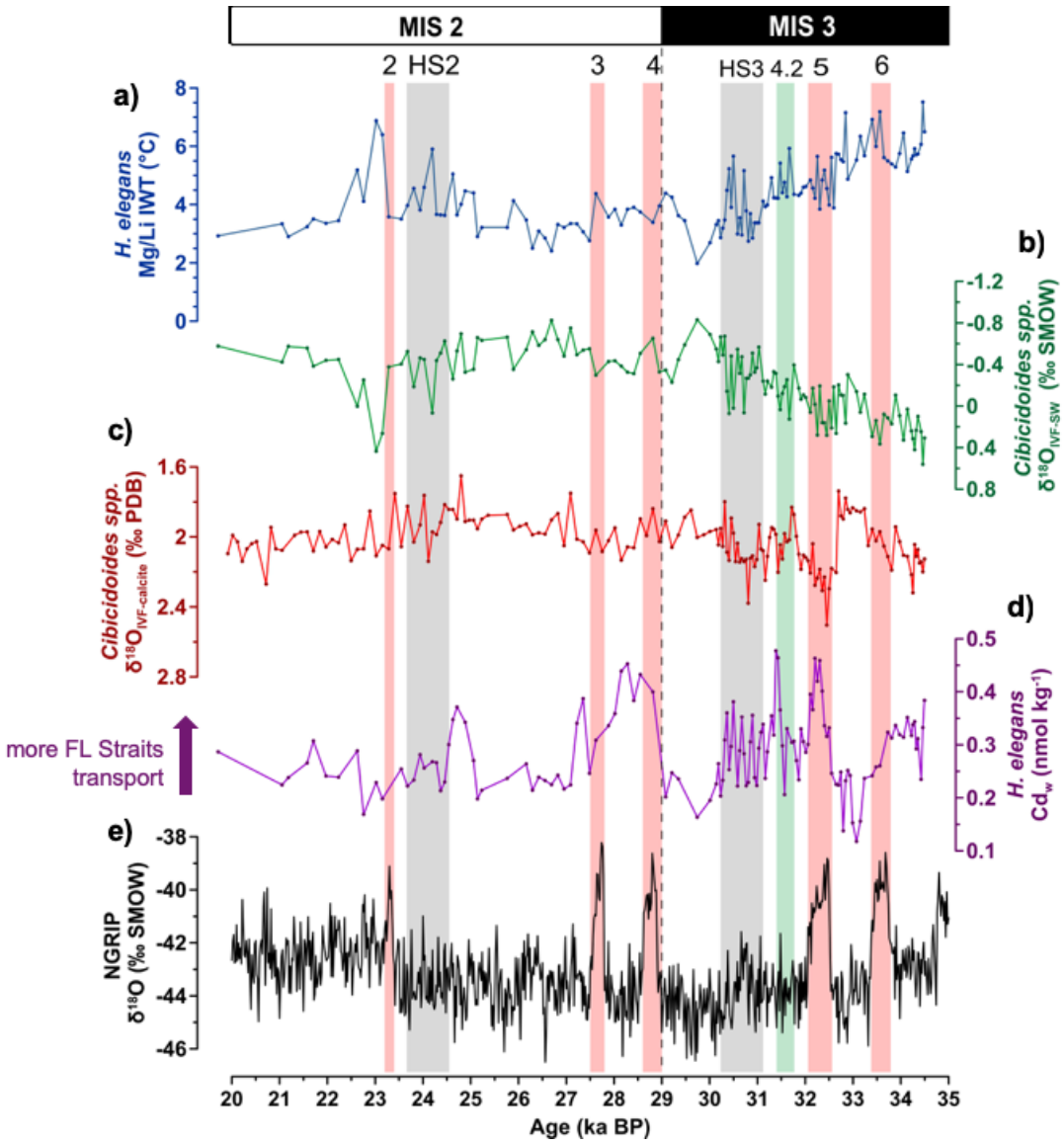

Figure 2-4 – Proxies as detailed in Fig. 2-3 (a-d), highlighting key stadial and interstadial intervals. MIS2 and late MIS3 are indicated in gray; D-O cycles, including D-O interstadials 2-6 and 4.2 as referenced in Them et al., 2015 are marked in pink and green. e) NGRIP $\delta^{18}O$ presented on its own age model (NGRIP members, 2004; Andersen et al., 2006). No further age model adjustments or peak alignments between NGRIP data and Florida Straits were made.

2.4.4 AMOC variability over Dansgaard-Oeschger events

Them et al. (2015), also using core KNR-166-2 26JPC, presented evidence of AMOC variability in the Florida Straits coincident with some Dansgaard-Oeschger (D-O) events, which manifest as rapid and brief warm periods in northern hemisphere climate records. This variability was inferred from the $\delta^{18}O$ record in benthic foraminifera, where heavy (cold) values were interpreted as more strongly tilted isopycnals and a stronger Florida Current during two warm events. This study also inferred decreased surface salinity during the interstadials due to the stronger AMOC and more northerly Intertropical Convergence Zone (ITCZ) in the Atlantic. However, unlike periods of abrupt climate change during deglaciation, the heavier $\delta^{18}O$ values are not reflected in lower Mg/Li temperature during the portion of this record in MIS 3 (~29-35 ka). The predominant trend for intermediate depth water at this location is a progressive decline into minimum glacial temperatures. This suggests that stadial increases in benthic foraminiferal $\delta^{18}O$ noted by Them et al. (2015) are driven instead by changes in seawater $\delta^{18}O$. If this is the case, this weakens the link between benthic foraminiferal $\delta^{18}O$ and AMOC change over this time interval.

Unlike the Florida Straits Mg/Li-derived temperature record, our record of Cd_W does provide support for the interpretation of Them et al. (2015) for enhanced AMOC during some D-O interstadials. Elevated Cd_w during D-O 5 aligns with peaks in the NGRIP record of $\delta^{18}O$ of Greenland ice (NGRIP members, 2004; Andersen et al., 2006), a proxy for northern hemisphere temperature, and in benthic foraminifera $\delta^{18}O$ from the KNR-166-2 26JPC core, supporting the interpretation of enhanced Florida Straits

throughflow strength (Lynch-Stieglitz et al., 1999; Them et al., 2015); see Fig. 2-4. While not present in the Greenland record, an additional interstadial (D-O 4.2) has been identified in surface water records from this core (Them et al., 2015) and is also visible in records of lower latitude hydrologic change (e.g. Peterson et al., 2000; Kanner et al., 2012). We also find an excursion to higher Cd_w values for this peak which would suggest AMOC strengthening, but as for the main D-O events, there is no indication of cooler temperature.

While a ~1.5 kyr peak in Cd_w around 28 ka may appear to indicate an extended AMOC reinvigoration associated with two brief D-O events (D-O interstadials 2 & 3), the lack of an obvious signal in benthic $\delta^{18}O$ of calcite, lower Mg/Li temperature, or lower inferred sea surface salinity (Them et al., 2015) make this interpretation more tenuous. It is also possible that excursions of elevated Cd_w over MIS2 arise from a different mechanism such as the ac- cumulation of respired nutrients in a poorly ventilated water mass of North Atlantic origin, although the lack of a commensurate signal in $\delta^{13}C$ during this period (Fig. 2-3e) is inconsistent with this hypothesis.

Overall, we are presented with inconsistent evidence for AMOC variability over the D-O events with some proxies indicating strengthening over some events, but not all proxies over all events. Despite this, there is a strong response in both Cd_w and $\delta^{18}O$ of benthic foraminiferal calcite over D-O 5, and we conclude that these signatures likely reflect changes in AMOC strength over this event.

2.5 Conclusions

Our Mg/Li-derived temperature record demonstrates the utility of a promising proxy for bottom water temperature. This record is consistent with modern Florida Straits bottom water temperature estimates. This study also shows temperature changes predicted by AMOC variability coincident with abrupt climate events on the deglaciation that were inferred based on records of Cd_w and $\delta^{18}O$ from the same sediment core. These findings confirm the hypothesis presented in earlier work in the Florida Straits that lower deglacial benthic $\delta^{18}O$ during deglacial stadial events primarily reflect intermediate water warming, not freshening (Lynch-Stieglitz et al., 2014). We also find some limited support from our Cd_w record for AMOC variability during Late MIS 3. These findings suggest that over the last ~35,000 yr, AMOC changes are linked to periods of abrupt climate change during the deglaciation, and possibly also during Late MIS 3.

In contrast to our ability to explain the variability in Florida Straits temperature, nutrients, and $\delta^{18}O_{SW}$ during periods of reduced ice volume (the deglaciation and Late MIS 3) in terms of differing contributions of the existing northern and southern sourced intermediate water masses, changes in the contributing end members are required to describe the LGM state. Additional subsurface and intermediate water Mg/Li-derived temperature records may help confirm whether the cold, fresh water in the glacial Florida Straits during the LGM is broadly representative of GNAIW, and help characterize the LGM circulation state.

2.6 Acknowledgements

We thank John Morton, Brigitta Rongstad, and Tiee-Yuh Chang for laboratory assistance. We also thank the reviewers for their helpful input. This work was funded by the NSF Graduate Research Fellowship DGE-1148903 (SV) and NSF grant OCE-1459563 (JLS). Data is archived in the NOAA National Centers for Environmental Information Paleoclimatology database: https://www.ncdc.noaa. gov/paleo- search/.

CHAPTER 3. SEAWATER-CADMIUM INFERRED UPPER AMOC VARIABILITY IN THE LATE COMMON ERA

3.1 Introduction

Atlantic meridional overturning circulation (AMOC) is a key component of the climate system, as it transfers heat from the Southern Hemisphere to the Northern Hemisphere. It has been implicated in the global expression of climate change, by forcing a "bipolar seesaw" of hemispheric temperatures (Broecker, 1998; Rahmstorf, 2002) and via processes that force shifts in the mean position of the intertropical convergence zone and monsoons (Chiang and Bitz, 2005; Vellinga and Wood, 2002; Zhang et al., 2005). Additionally, AMOC transports heat and carbon from the surface to the interior ocean (Kostov et al., 2014; Marshall et al., 2014), and may help determine the pace and patterns of warming due to the release of anthropogenic carbon. For these reasons, characterizing AMOC variability over many different timescales is key to understanding its current and future behavior and resulting climate impacts.

Evidence of AMOC decline over the late twentieth century was inferred from North Atlantic sea surface temperature data (Rahmstorf et al., 2015a) and from partial records of circulation and sea surface height (Mercier et al., 2015). Since then, observational arrays that capture continuous measurements of northward and southward flow across the Atlantic basin have come online (Lozier et al., 2019; Srokosz and Bryden, 2015). A decade of measurements from the RAPID array at 26.5 N confirmed an AMOC in decline since 2008, though the extent to which this trend is related to Atlantic Multidecadal Variability/Atlantic Multidecadal Oscillation (AMV/AMO), decadal variability, and

anthropogenic warming is undiscernible from the abbreviated record (Smeed et al., 2018). Models also project continued AMOC decline through 2100, but rates and magnitudes of weakening vary greatly depending on the model's climate sensitivity and the projected AMOC variability (IPCC, 2013). In light of the uncertainty around multidecadal AMOC variability and projections of future AMOC, paleoceanographic reconstructions seek to place AMOC variability over the last decades within the context of variability over the last centuries.

Attempts to characterize AMOC variability in the pre-modern Common Era have yielded mixed findings. Lund et al. (Lund et al., 2006) applied the geostrophic method using benthic $\delta^{18}O$ measurements to estimate Gulf Stream transport in the Florida Straits, a component of upper branch AMOC. They estimated that this transport was 10% weaker during the Little Ice Age (LIA, ~1200-1850 CE) but has since recovered in the last ~150 years before present. By inferring AMOC changes from proxies recording western boundary current transport and upper ocean heat content, Thornalley et al. (2018) found that since the LIA (here cited as ~1350-1850 CE), AMOC has been weaker relative to the past 1,500 years. They conclude that AMOC has not recovered after the LIA but has instead been anomalously weak in the last ~150 years before present.

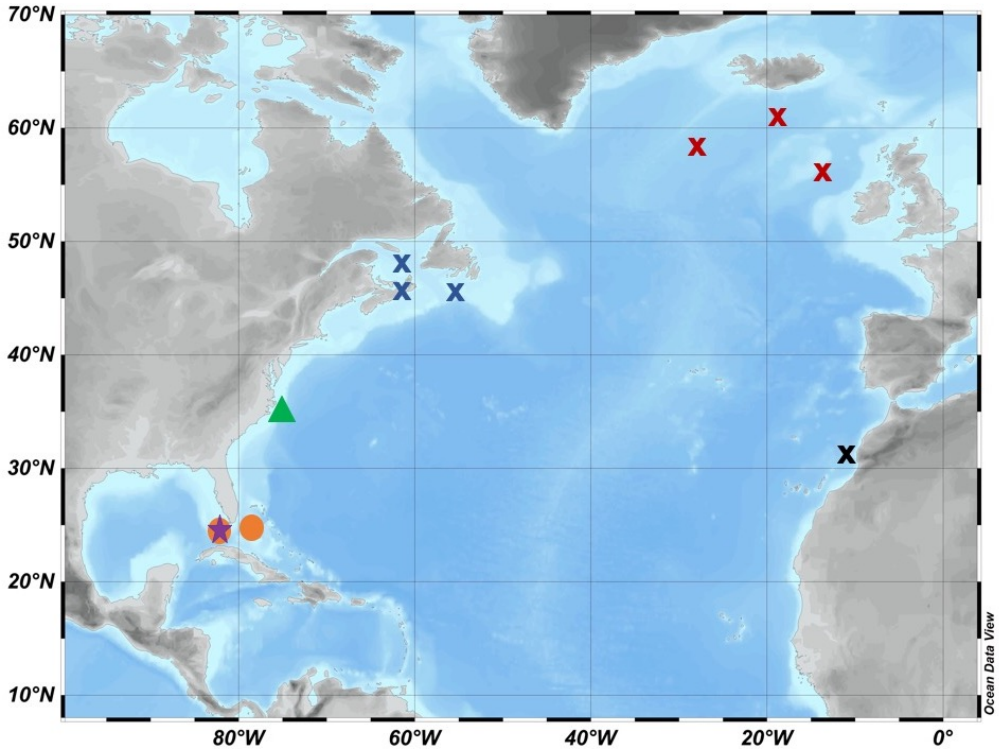

Figure 3-1 – Locations of Common Era AMOC reconstructions. All locations are approximate; full core information from this study are included in Appendices D and E. Star: cores used for Cd_w reconstruction: KNR166-2 3MC-H, KNR166-2 62MC-A, W167-79GGC, this study and KNR166-2 26 JPC, Valley et al., 2017. Circles: cores used in the Lund et al., 2006 density gradient-based reconstruction of Gulf Stream transport. Triangle, cores used in Thornalley et al., 2018 sortable silt reconstruction of deep western boundary current flow. X symbols show the subsurface temperature proxy sites applied in Thornalley et al., 2018, where red and blue symbols indicate areas in a dipole where subsurface ocean heat temperature warms and cools, respectively, with strengthened AMOC.

In this study, we revisit the Florida Straits transport characterization using the Cd/Ca tracer to infer upper AMOC change over the last 1,000 years. Bottom waters (which are of intermediate ocean depth) in the Florida Straits are comprised of both fresher, higher nutrient waters from the South Atlantic and saltier, lower nutrient from the North Atlantic subtropical gyre. Since the throughflow of southern water is indicative of upper branch AMOC transport, the nutrient water mass tracer seawater Cd (Cd_w) can be applied to

infer AMOC variability as in (Came et al., 2008; Valley et al., 2017; 2019). We also derive temperature from Mg/Li measured in the same cores in order to compare our analyses to Florida Straits density estimates.

3.2 Methods

Three of the Florida Straits cores included in the Lund et al. 2006 study were analyzed for trace and minor metal content (Fig. 3-1). These sites were selected to include those cores retrieved from below 400 m depth, which are the depths that include waters incorporating nutrient levels reflective of both the presence of southern-sourced Antarctic Intermediate Water (AAIW) and remineralization in tropical waters south of the Florida Straits. Each core also has a modern core top; age models are applied as in (Lund et al., 2006; Lund and Curry, 2006; 2004), but raw ^{14}C values are converted to calendar ages using CALIB 7.1. The cores range in water depth 447-694 m and have average sedimentation rates 20-33 cm/kyr.

Cd/Ca, Mg/Ca, and Li/Ca ratios were measured in the tests of the benthic foraminifer *Hoeglundina elegans*, after cleaning using the reductive and oxidative procedures outlined by Boyle and Kegwin (Boyle and Keigwin, 1985) and modified by Boyle and Rosenthal (Boyle and Rosenthal, 1996).We analyzed 1 to 20 >250 μm individual foraminifera per sample (samples containing more than 10 foraminifera were homogenized, split and analyzed separately) on a Thermo Finnigan Element2 magnetic sector inductively coupled plasma-mass spectrometer using the methods of Marchitto

(Marchitto, 2006). Analytical precision (1σ) is 2% for Cd/Ca, 0.5% for Mg/Ca, 0.9%, and Li/Ca (Bryan and Marchitto, 2008).

As the partitioning of Cd in *H. elegans* is not strongly depth dependent, Cd_w was calculated from Cd/Ca using a partition coefficient of 1 (Boyle et al., 1995) and an assumed global mean seawater Ca concentration 0.01 $molkg^{-1}$ (Boyle, 1992).

Because of the scarcity of Common Era samples, Cd_w and Mg/Li data from the three nearby cores in the Dry Tortugas are combined for analysis. Of 109 samples analyzed (including replicates), eleven Mg/Li measurements are discarded due to Li contamination in the sample dissolving acid. Eight Cd_w and four temperature data points are excluded as outliers, identified using the function smooth.m (Matlab version R2017b) with a robust Lowess smoothing method and 10% data smoothing window. Data beyond 2σ of the smoothed time series were marked as outliers.

Temperatures were reconstructed from Mg/Li ratios using the empirically derived polynomial calibration equation for *H. elegans*:

$$Mg/Li = 0.150 \pm 0.012 + 0.0209 \pm 0.0027T - 0.0002 \pm 0.0001\ T^2$$

(Marchitto et al., 2018). The equation's fit corresponds to $r^2 = 0.95$, and 1σ standard error for Mg/Li is 0.022 mol $mmol^{-1}$, equivalent to ±1.0°C at 0°C and ±1.7°C at 20°C.

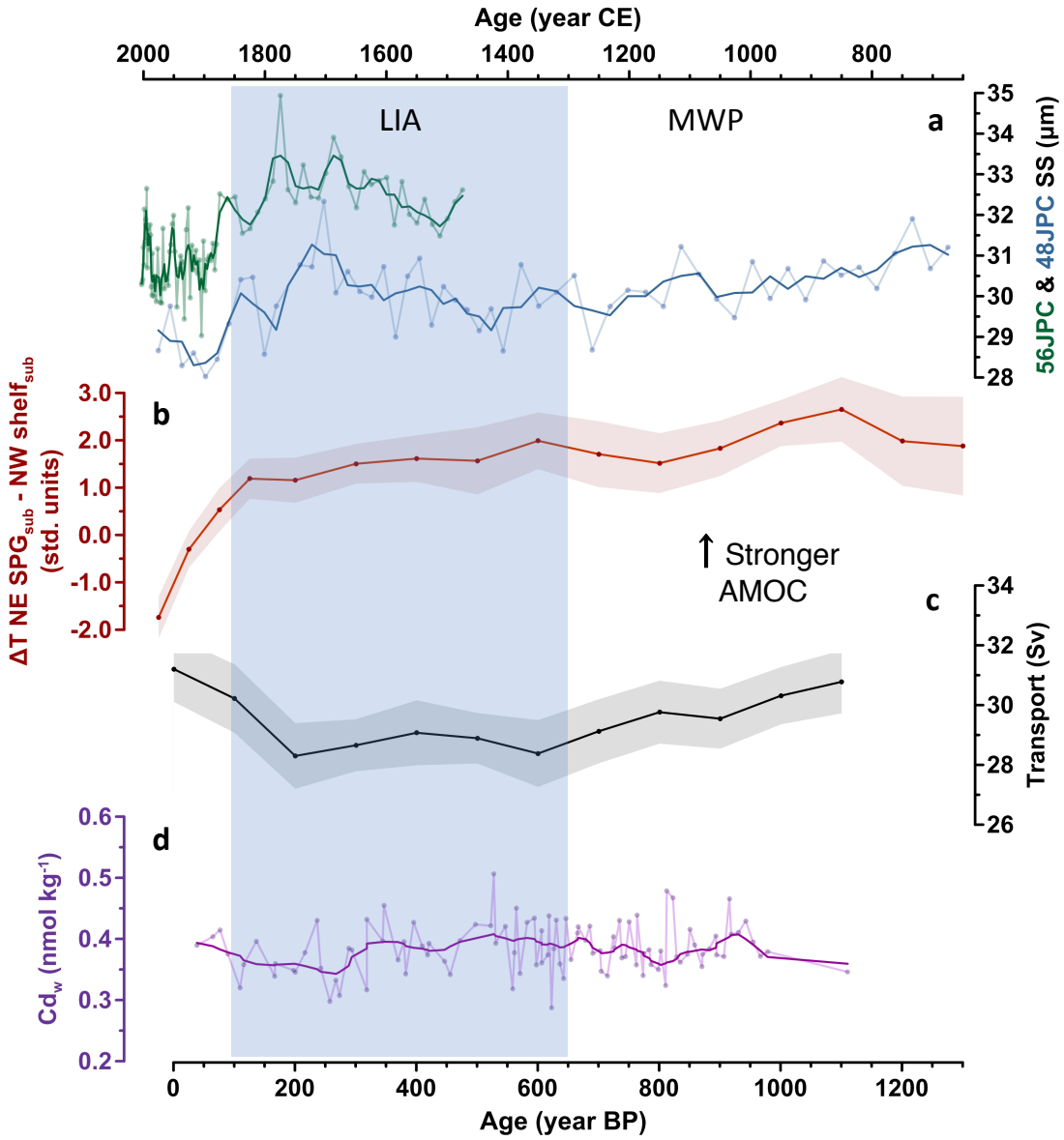

Figure 3-2 – Paleo proxy AMOC reconstructions. For each proxy, stronger AMOC is up and weaker AMOC is down. (a) Mean grain size sortable silt (SS) with three-point means (bold curve) and (b), T_{sub} AMOC index, both from Thornalley et al., 2018. (b) is constructed following the methods of Zhang et al., 2008. (c), Transport (Sv) estimate from Florida Straits density-gradient analysis, Lund et al., 2006, (d), Seawater cadmium, this study.

3.3 Results and Discussion

Florida Straits Cd_w averaged 0.385 nmol kg^{-1} over the last 1100 years (Fig. 3-2(d)). During the LIA, Cd_w was 0.007 nmol kg^{-1} lower than in the Medieval Warm Period (~950-1250 CE). This does not suggest a reduction in AMOC during the LIA, as the difference between these periods is not statistically significant (2σ). The Cd_w reduction during this period, compared to the record preceding the MWP, is approximately one order of magnitude smaller than the decrease in Florida Straits Cd_w over the Younger Dryas, a cold period associated with weakened AMOC (Valley et al., 2017). This relatively small change between the MWP and LIA is consistent with Florida Straits density gradient changes during the LIA reported by Lund et al. (2006) being approximately one-tenth of those observed over the Younger Dryas (Lynch-Stieglitz et al., 2011). Mg/Li-derived temperatures remained relatively stable over the record, with an average of 6.6°C (Fig. 3). While a 2°C warming was associated with weakened Florida Straits transport during the Younger Dryas, the relative stability of temperatures in the combined Florida Straits core records underscores the subtlety of any changes in AMOC over the last ~1100 years. Average Cd_w after the LIA (since 1850 CE, or within 100 years BP) is also not significantly different from during the LIA, though our industrial era data are sparser. We refrain from drawing conclusions on AMOC in the post-LIA period due to the relatively low number of samples analyzed.

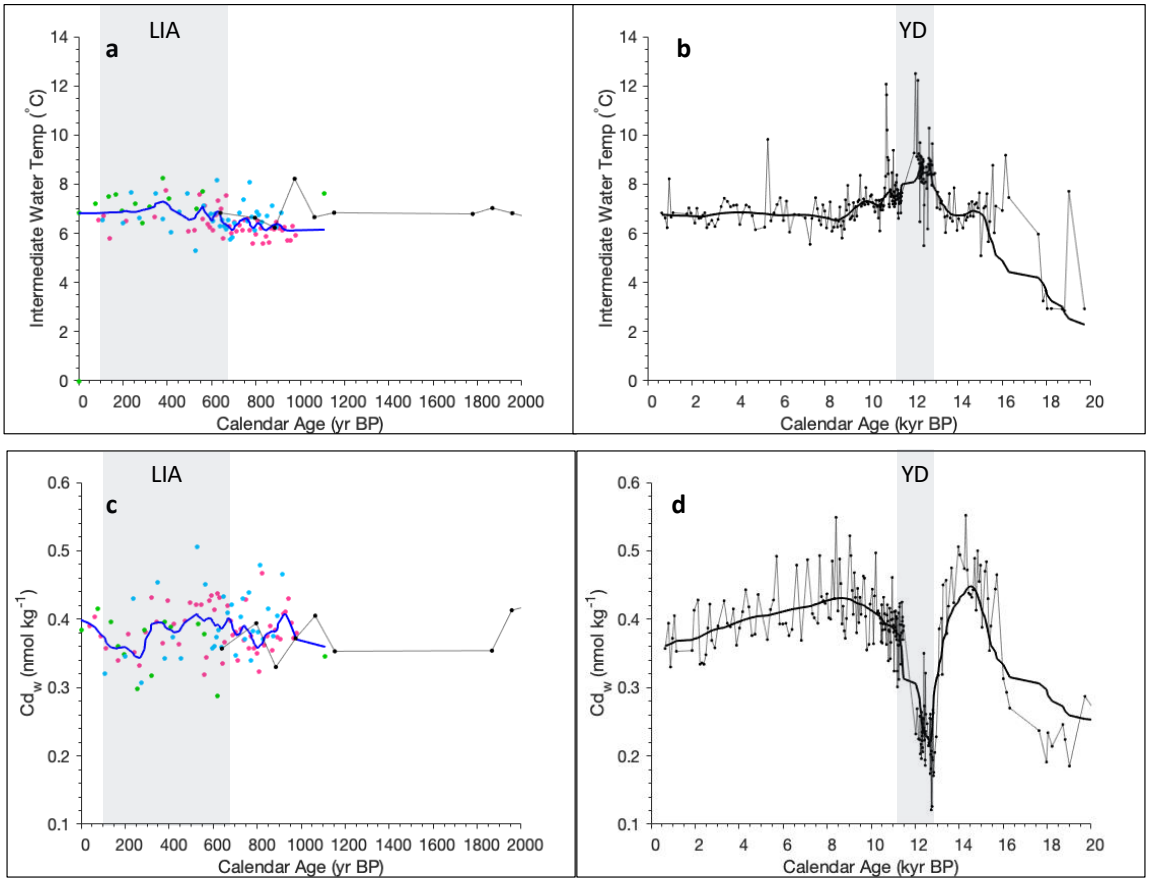

Figure 3-3 – Florida Straits temperature reconstructed from benthic Mg/Li. (a), Common Era temperatures from KNR 166-2 62MCA (pink), KNR 166-2 MC3H (green), and W167 79GGC (blue). The bolded blue curve shows a 10% robust Lowess smoothing of the combined data. The black line is a subsection of the deeper time record from core KNR166-2 26JPC (Valley et al., 2019). (b) The deeper time record showing a larger temperature increase during the AMOC slowdown of the Younger Dryas. (c) and (d), similar reconstructions of Cd_w from the combined Florida Straits cores (colors as in (a)), and KNR166-2 26JPC (black).

A potential source of difference between AMOC estimates in the Florida Straits and those captured further north in the Atlantic, as in Thornalley et al. (2018), is meridional incoherence of the AMOC. The dominant mechanisms for overturning variability depend on timescale. Regionally variable wind-driven processes dominate on intra-annual to interannual timescales (Xu et al., 2014; Zhao and Johns, 2014), while buoyancy-driven processes that are more coherent across latitudes play a larger role in forcing AMOC

variability on decadal and longer timescales (Buckley et al., 2012; Tulloch and Marshall, 2012). Accordingly, modelling and observational studies have found that AMOC is not coherent between the North Atlantic subpolar and subtropical gyres on interannual to decadal timescales (Bingham et al., 2007; Lozier et al., 2010; Mielke et al., 2013; Roussenov et al., 2014). However, a model study specifically comparing Florida Current transport to integrated AMOC transport finds them highly correlated on decadal or longer timescales, particularly near the region of our study (24°N) (Sifan Gu, personal communication). The multidecadal resolution of our cores justifies their analysis in comparison to other Common Era reconstructions of AMOC.

The Florida Straits Common Era Cd_w record agrees with AMOC proxy records from other latitudes in the North Atlantic (Lund et al., 2006; Rahmstorf et al., 2015b; Thornalley et al., 2018) that show a stable or slightly weakening AMOC during the LIA relative to the MWP, demonstrating the meridional coherence of AMOC over decadal to multidecadal timescales. Yet still unresolved is the disagreement between post-LIA records from the Florida Straits showing an AMOC recovery of ~2 Sv (Lund et al., 2006)- of similar magnitude to decadal AMOC variability- and records from the subpolar and subtropical regions further north showing a decline of AMOC around the same magnitude or greater (Rahmstorf et al., 2015b; Thornalley et al., 2018). Given the high interannual variability of AMOC and its meridional coherence's dependency on timescale, more paleo-reconstructions from the recent past should be made using additional tracers and sampling strategies that carefully consider the resolution of the AMOC reconstructions.

3.4 Conclusions

Given observations in the paleorecord of reduced AMOC during periods of cold temperatures and freshwater influxes in the North Atlantic, it is notable that several Common Era AMOC reconstructions show a distinct AMOC slowdown *following* the Little Ice Age. The Florida Straits records highlight the subtlety of AMOC changes across centennial-scale climate shifts. These findings underscore the need for greater understanding of AMOC's stability and under what conditions AMOC changes may lead or lag shifts in climate. These questions remain highly relevant in the current period of rapidly melting Arctic ice.

3.5 Acknowledgements

I thank my collaborators Jean Lynch-Stieglitz and Tom Marchitto, as well as Delia Oppo, David Lund, and technician John Morton, for their input and assistance in laboratory analysis.

APPENDIX A. CD/CA AND CD_W FROM CORE KNR166-2 26 JPC

Outliers beyond 2 standard deviations of a Lowess smoothed time series are indicated as 1 and omitted from interpretation.

Depth (cm)	Calendar Age (yr BP)	Cd/Ca (umol mol^{-1})	Cd_w (nmol kg^{-1})	Flagged Outlier
0.75	640	0.0357	0.357	
4.25	796	0.0394	0.394	
6.25	885	0.0330	0.330	
8.25	975	0.0372	0.372	
10.25	1064	0.0405	0.405	
12.25	1153	0.0353	0.353	
26.25	1778	0.0632	0.632	1
28.25	1867	0.0354	0.354	
30.25	1957	0.0413	0.413	
34.25	2135	0.0428	0.428	
36.25	2224	0.0334	0.334	
38.25	2314	0.0336	0.336	
40.25	2403	0.0334	0.334	
42.25	2492	0.0348	0.348	
44.25	2581	0.0387	0.387	
46.26	2671	0.0422	0.422	
48.25	2760	0.0369	0.369	
50.25	2900	0.0358	0.358	
52.25	3041	0.0390	0.390	
54.25	3181	0.0348	0.348	1
56.25	3321	0.0427	0.427	
58.25	3462	0.0394	0.394	
60.25	3602	0.0389	0.389	
62.25	3742	0.0415	0.415	
64.25	3883	0.0362	0.362	
66.25	4023	0.0387	0.387	
68.25	4163	0.0411	0.411	
70.25	4303	0.0443	0.443	
72.25	4444	0.0418	0.418	
74.25	4584	0.0376	0.376	
76.25	4724	0.0378	0.378	
78.25	4865	0.0436	0.436	
84.25	5286	0.0370	0.370	

Depth (cm)	Calendar Age (yr BP)	Cd/Ca (umol mol^{-1})	Cd_w (nmol kg^{-1})	Flagged Outlier
86.25	5426	0.0414	0.414	
88.25	5566	0.0428	0.428	
90.25	5707	0.0492	0.492	
92.25	5847	0.0393	0.393	
94.25	5987	0.0393	0.393	
96.25	6128	0.0394	0.394	
98.25	6268	0.0376	0.376	
100.25	6408	0.0385	0.385	
103.25	6619	0.0479	0.479	
106.25	6829	0.0369	0.369	
110.25	7110	0.0487	0.487	
114.25	7333	0.0408	0.408	
116.25	7415	0.0402	0.402	
120.25	7580	0.0394	0.394	
122.25	7663	0.0493	0.493	
124.25	7745	0.0433	0.433	
126.25	7828	0.0427	0.427	
128.25	7910	0.0423	0.423	
130.25	7993	0.0437	0.437	
132.25	8075	0.0402	0.402	
134.25	8158	0.0400	0.400	
136.25	8240	0.0485	0.485	
138.25	8323	0.0430	0.430	
140.25	8405	0.0549	0.549	
142.25	8488	0.0412	0.412	
144.25	8570	0.0488	0.488	
146.25	8621	0.0452	0.452	
148.25	8673	0.0393	0.393	
150.25	8724	0.0419	0.419	
152.25	8775	0.0383	0.383	
154.25	8826	0.0372	0.372	
156.25	8878	0.0401	0.401	
158.25	8929	0.0303	0.303	1
160.25	8980	0.0623	0.623	1
162.25	9032	0.0522	0.522	
164.25	9083	0.0493	0.493	
166.25	9134	0.0442	0.442	
168.25	9185	0.0407	0.407	

Depth (cm)	Calendar Age (yr BP)	Cd/Ca (umol mol^{-1})	Cd_w (nmol kg^{-1})	Flagged Outlier
170.25	9237	0.0468	0.468	
172.25	9288	0.0432	0.432	
174.25	9339	0.0380	0.380	
176.25	9390	0.0445	0.445	
178.25	9442	0.0395	0.395	
180.25	9493	0.0432	0.432	
182.25	9544	0.0407	0.407	
184.25	9596	0.0277	0.277	1
186.25	9647	0.0463	0.463	
188.25	9698	0.0460	0.460	
190.25	9749	0.0404	0.404	
192.25	9801	0.0355	0.355	
194.25	9852	0.0544	0.544	1
196.25	9903	0.0363	0.363	
198.25	9955	0.0422	0.422	
202.25	10057	0.0444	0.444	
204.25	10108	0.0364	0.364	
206.25	10160	0.0434	0.434	
208.25	10211	0.0497	0.497	
210.25	10262	0.0409	0.409	
212.25	10313	0.0412	0.412	
214.25	10365	0.0408	0.408	
216.25	10416	0.0401	0.401	
218.25	10438	0.0394	0.394	
220.25	10459	0.0367	0.367	
222.25	10481	0.0421	0.421	
224.25	10503	0.0365	0.365	
226.25	10524	0.0384	0.384	
228.25	10546	0.0393	0.393	
230.25	10568	0.0432	0.432	
234.25	10611	0.0408	0.408	
236.25	10633	0.0385	0.385	
238.25	10655	0.0393	0.393	
242.25	10698	0.0363	0.363	
244.25	10720	0.0406	0.406	
246.25	10741	0.0421	0.421	
248.25	10763	0.0397	0.397	
250.25	10785	0.0339	0.339	

Depth (cm)	Calendar Age (yr BP)	Cd/Ca (umol mol^{-1})	Cd_w (nmol kg^{-1})	Flagged Outlier
252.25	10806	0.0384	0.384	
254.25	10828	0.0382	0.382	
256.25	10850	0.0416	0.416	
258.25	10871	0.0342	0.342	
260.25	10893	0.0366	0.366	
262.25	10915	0.0399	0.399	
264.25	10937	0.0410	0.410	
266.25	10958	0.0461	0.461	
268.25	10980	0.0400	0.400	
270.25	11002	0.0391	0.391	
272.25	11023	0.0381	0.381	
274.25	11045	0.0324	0.324	
276.25	11067	0.0411	0.411	
278.25	11088	0.0388	0.388	
280.25	11110	0.0412	0.412	
282.25	11122	0.0375	0.375	
284.25	11134	0.0383	0.383	
286.25	11147	0.0404	0.404	
288.25	11159	0.0370	0.370	
290.25	11171	0.0401	0.401	
292.25	11183	0.0324	0.324	
294.25	11196	0.0301	0.301	
298.25	11220	0.0362	0.362	
302.25	11244	0.0409	0.409	
304.25	11257	0.0312	0.312	
306.25	11269	0.0362	0.362	
308.25	11281	0.0369	0.369	
310.25	11293	0.0418	0.418	
312.25	11306	0.0423	0.423	
314.25	11318	0.0392	0.392	
316.25	11330	0.0376	0.376	
319.25	11348	0.0334	0.334	
324.25	11379	0.0380	0.380	
326.25	11391	0.0392	0.392	
328.25	11403	0.0425	0.425	
330.25	11416	0.0397	0.397	
332.25	11428	0.0403	0.403	
334.25	11440	0.0370	0.370	

Depth (cm)	Calendar Age (yr BP)	Cd/Ca (umol mol^{-1})	Cd_w (nmol kg^{-1})	Flagged Outlier
336.25	11452	0.0383	0.383	
340.25	11477	0.0390	0.390	
430.25	12027	0.0232	0.232	
440.25	12088	0.0269	0.269	
448.25	12149	0.0225	0.225	
454.25	12198	0.0224	0.224	
456.25	12215	0.0258	0.258	
458.25	12231	0.0203	0.203	
462.25	12264	0.0217	0.217	
464.25	12280	0.0385	0.385	1
466.25	12287	0.0196	0.196	
468.25	12294	0.0264	0.264	
472.25	12307	0.0222	0.222	
474.25	12314	0.0235	0.235	
476.25	12321	0.0229	0.229	
478.25	12327	0.0248	0.248	
480.25	12334	0.0212	0.212	
484.25	12348	0.0206	0.206	
486.25	12354	0.0234	0.234	
488.25	12361	0.0255	0.255	
492.25	12375	0.0254	0.254	
496.25	12388	0.0238	0.238	
498.25	12395	0.0350	0.350	
500.25	12402	0.0241	0.241	
504.25	12415	0.0273	0.273	
506.25	12422	0.0223	0.223	
508.25	12429	0.0236	0.236	
512.25	12442	0.0232	0.232	
514.25	12449	0.0194	0.194	
516.25	12456	0.0186	0.186	
518.25	12462	0.0236	0.236	
520.25	12469	0.0321	0.321	
524.25	12483	0.0261	0.261	
542.25	12543	0.0247	0.247	
548.25	12576	0.0227	0.227	
552.25	12602	0.0215	0.215	
556.25	12628	0.0219	0.219	
558.25	12640	0.0215	0.215	

Depth (cm)	Calendar Age (yr BP)	Cd/Ca (umol mol^{-1})	Cd_w (nmol kg^{-1})	Flagged Outlier
562.25	12666	0.0255	0.255	
564.25	12679	0.0174	0.174	
566.25	12692	0.0261	0.261	
568.25	12705	0.0202	0.202	
570.25	12718	0.0181	0.181	
572.25	12731	0.0121	0.121	
574.25	12744	0.0207	0.207	
576.25	12757	0.0254	0.254	
578.25	12770	0.0126	0.126	
580.25	12783	0.0198	0.198	
582.25	12795	0.0194	0.194	
584.25	12808	0.0267	0.267	
586.25	12821	0.0263	0.263	
588.25	12834	0.0171	0.171	
590.25	12847	0.0176	0.176	
594.25	12893	0.0205	0.205	
598.25	12959	0.0228	0.228	
604.25	13058	0.0318	0.318	
606.25	13091	0.0386	0.386	
612.25	13197	0.0401	0.401	
614.25	13232	0.0319	0.319	
616.25	13267	0.0450	0.450	
624.25	13408	0.0457	0.457	
626.25	13443	0.0379	0.379	
630.25	13513	0.0419	0.419	
636.25	13619	0.0249	0.249	1
638.25	13654	0.0475	0.475	
644.25	13760	0.0424	0.424	
648.25	13830	0.0633	0.633	1
652.25	13964	0.0506	0.506	
654.25	14031	0.0494	0.494	
660.25	14233	0.0474	0.474	
662.25	14300	0.0552	0.552	
664.25	14367	0.0472	0.472	
666.25	14434	0.0438	0.438	
668.25	14501	0.0436	0.436	
670.25	14569	0.0432	0.432	
672.25	14636	0.0443	0.443	

Depth (cm)	Calendar Age (yr BP)	Cd/Ca (umol mol^{-1})	Cd_w (nmol kg^{-1})	Flagged Outlier
674.25	14703	0.0489	0.489	
676.25	14770	0.0413	0.413	
678.25	14837	0.0500	0.500	
680.25	14904	0.0455	0.455	
682.25	14971	0.0479	0.479	
684.25	15039	0.0388	0.388	
688.25	15173	0.0470	0.470	
690.25	15240	0.0484	0.484	
692.25	15307	0.0430	0.430	
694.25	15374	0.0354	0.354	
696.25	15441	0.0390	0.390	
700.25	15576	0.0274	0.274	1
702.25	15643	0.0444	0.444	
704.25	15710	0.0465	0.465	
708.25	16006	0.0313	0.313	
710.25	16154	0.0293	0.293	
712.25	16301	0.0270	0.270	
730.25	17632	0.0237	0.237	
734.25	17843	0.0417	0.417	1
738.25	17969	0.0191	0.191	
740.25	18032	0.0234	0.234	
746.25	18221	0.0214	0.214	
758.25	18711	0.0246	0.246	
760.25	18812	0.0224	0.224	
764.25	19012	0.0185	0.185	
778.25	19715	0.0287	0.287	
804.25	21051	0.0224	0.224	
806.25	21183	0.0238	0.238	
808.25	21314	0.0752	0.752	1
812.25	21577	0.0266	0.266	
814.25	21708	0.0307	0.307	
818.25	21970	0.0241	0.241	
822.25	22233	0.0239	0.239	
828.25	22627	0.0289	0.289	
830.25	22758	0.0169	0.169	
834.25	23021	0.0229	0.229	
836.25	23152	0.0198	0.198	
838.25	23283	0.0426	0.426	1

Depth (cm)	Calendar Age (yr BP)	Cd/Ca (umol mol^{-1})	Cd_w (nmol kg^{-1})	Flagged Outlier
842.25	23546	0.0254	0.254	
844.25	23677	0.0222	0.222	
846.25	23809	0.0234	0.234	
848.25	23940	0.0281	0.281	
850.25	24026	0.0256	0.256	
854.25	24198	0.0268	0.268	
856.25	24284	0.0266	0.266	
858.25	24370	0.0213	0.213	
860.25	24456	0.0230	0.230	
862.25	24542	0.0300	0.300	
864.25	24628	0.0347	0.347	
866.25	24714	0.0371	0.371	
868.25	24800	0.0222	0.222	1
870.25	24886	0.0342	0.342	
874.25	25058	0.0270	0.270	
876.25	25144	0.0198	0.198	
878.25	25230	0.0214	0.214	
886.25	25761	0.0237	0.237	
888.25	25894	0.0426	0.426	1
892.25	26159	0.0264	0.264	
894.25	26292	0.0214	0.214	
896.25	26424	0.0239	0.239	
898.25	26557	0.0233	0.233	
900.25	26690	0.0225	0.225	
902.25	26822	0.0242	0.242	
904.25	26955	0.0217	0.217	
906.25	27088	0.0224	0.224	
908.25	27221	0.0340	0.340	
910.25	27353	0.0387	0.387	
912.25	27486	0.0246	0.246	
914.25	27619	0.0309	0.309	
918.25	27884	0.0336	0.336	
920.25	28017	0.0359	0.359	
922.25	28149	0.0439	0.439	
924.25	28282	0.0453	0.453	
926.25	28415	0.0383	0.383	
928.25	28548	0.0432	0.432	
932.25	28813	0.0400	0.400	

Depth (cm)	Calendar Age (yr BP)	Cd/Ca (umol mol^{-1})	Cd_w (nmol kg^{-1})	Flagged Outlier
934.25	28946	0.0596	0.596	1
936.25	29078	0.0202	0.202	
938.25	29211	0.0247	0.247	
940.25	29344	0.0236	0.236	
942.25	29476	0.0373	0.373	1
946.25	29742	0.0163	0.163	
950.25	30007	0.0195	0.195	
952.25	30140	0.0226	0.226	
954.25	30185	0.0264	0.264	
956.25	30229	0.0203	0.203	
958.25	30274	0.0233	0.233	
960.25	30318	0.0309	0.309	
962.25	30363	0.0360	0.360	
964.25	30407	0.0253	0.253	
966.25	30452	0.0297	0.297	
968.25	30496	0.0381	0.381	
970.25	30541	0.0654	0.654	1
972.25	30585	0.0222	0.222	
974.25	30630	0.0289	0.289	
976.25	30674	0.0352	0.352	
978.25	30719	0.0283	0.283	
980.25	30763	0.0222	0.222	
982.25	30808	0.0229	0.229	
984.25	30852	0.0305	0.305	
986.25	30897	0.0356	0.356	
988.25	30941	0.0238	0.238	
990.25	30986	0.0223	0.223	
992.25	31030	0.0293	0.293	
994.25	31075	0.0323	0.323	
996.25	31119	0.0338	0.338	
998.25	31164	0.0237	0.237	
1000.25	31208	0.0287	0.287	
1002.25	31253	0.0678	0.678	1
1004.25	31297	0.0355	0.355	
1006.25	31342	0.0318	0.318	
1008.25	31386	0.0477	0.477	
1010.25	31431	0.0464	0.464	
1012.25	31475	0.0366	0.366	

Depth (cm)	Calendar Age (yr BP)	Cd/Ca (umol mol^{-1})	Cd_w (nmol kg^{-1})	Flagged Outlier
1014.25	31520	0.0298	0.298	
1016.25	31569	0.0206	0.206	
1018.25	31618	0.0330	0.330	
1020.25	31667	0.0156	0.156	1
1022.25	31716	0.0304	0.304	
1024.25	31765	0.0307	0.307	
1026.25	31814	0.0271	0.271	
1028.25	31863	0.0234	0.234	
1030.25	31912	0.0330	0.330	
1032.25	31961	0.0306	0.306	
1034.25	32010	0.0286	0.286	
1036.25	32059	0.0301	0.301	
1038.25	32108	0.0395	0.395	
1040.25	32157	0.0366	0.366	
1042.25	32206	0.0463	0.463	
1044.25	32255	0.0420	0.420	
1046.25	32304	0.0459	0.459	
1048.25	32353	0.0401	0.401	
1050.25	32402	0.0336	0.336	
1052.25	32451	0.0316	0.316	
1054.25	32500	0.0332	0.332	
1056.25	32549	0.0246	0.246	
1058.25	32598	0.0364	0.364	1
1060.25	32647	0.0225	0.225	
1062.25	32696	0.0224	0.224	
1064.25	32745	0.0248	0.248	
1066.25	32794	0.0138	0.138	
1068.25	32843	0.0232	0.232	
1070.25	32892	0.0252	0.252	
1072.25	32941	0.0242	0.242	
1074.25	32990	0.0153	0.153	
1076.25	33072	0.0118	0.118	
1078.25	33154	0.0156	0.156	
1080.25	33236	0.0236	0.236	
1084.25	33400	0.0242	0.242	
1086.25	33482	0.0258	0.258	
1088.25	33564	0.0260	0.260	
1090.25	33646	0.0428	0.428	

Depth (cm)	Calendar Age (yr BP)	Cd/Ca (umol mol^{-1})	Cd_w (nmol kg^{-1})	Flagged Outlier
1092.25	33728	0.0324	0.324	
1094.25	33810	0.0313	0.313	
1096.25	33892	0.0337	0.337	
1098.25	33974	0.0319	0.319	
1100.25	34056	0.0314	0.314	
1102.25	34138	0.0351	0.351	
1104.25	34220	0.0317	0.317	
1106.25	34254	0.0338	0.338	
1108.25	34289	0.0344	0.344	
1110.25	34323	0.0292	0.292	
1112.25	34357	0.0311	0.311	
1116.25	34426	0.0235	0.235	
1118.25	34460	0.0332	0.332	
1120.25	34494	0.0384	0.384	

APPENDIX B. LI/CA, MG/CA, MG/LI, AND MG/LI-DERIVED TEMPERATURE FROM CORE KNR166-2 26 JPC

Outliers beyond 2 standard deviations of a Lowess smoothed time series are indicated as 1 and omitted from interpretation.

Depth (cm)	Calendar Age (yr BP)	Li/Ca	Mg/Ca	Mg/Li (mol mmol^{-1})	Mg/Li T (°C)	Flagged Outlier
0.75	640	3.66662742	1.03941693	0.283	6.83	
4.25	796	3.82347486	1.06979244	0.280	6.63	
6.25	885	3.80780064	1.03724551	0.272	6.23	
8.25	975	3.84634437	1.1858343	0.308	8.22	
10.25	1064	3.93718056	1.10368096	0.280	6.66	
12.25	1153	3.67179234	1.04119123	0.284	6.84	
26.25	1778	3.6371804	1.02817657	0.283	6.79	
28.25	1867	3.68604568	1.05778925	0.287	7.03	
30.25	1957	3.7440258	1.06016123	0.283	6.82	
34.25	2135	3.63935425	1.00429356	0.276	6.42	
36.25	2224	3.76414905	1.08012563	0.287	7.02	
38.25	2314	3.65233106	1.02037419	0.279	6.61	
40.25	2403	3.92451607	1.09822536	0.280	6.63	
42.25	2492	3.95014788	1.11231421	0.282	6.73	
44.25	2581	4.01791944	1.13929011	0.284	6.84	
46.26	2671	3.87440211	1.05532358	0.272	6.23	
48.25	2760	4.18019992	1.14967116	0.275	6.37	
50.25	2900	4.4158787	1.22727163	0.278	6.53	
52.25	3041	3.77243299	1.03118803	0.273	6.28	
54.25	3181	3.92102998	1.09264896	0.279	6.57	
56.25	3321	3.8739784	1.11649148	0.288	7.09	
58.25	3462	3.99488478	1.17557299	0.294	7.43	
60.25	3602	3.69477758	1.07877665	0.292	7.30	
62.25	3742	3.99899771	1.15184354	0.288	7.08	
64.25	3883	3.5004055	1.01183355	0.289	7.14	
66.25	4023	3.51210982	1.01559662	0.289	7.15	
68.25	4163	3.59779074	0.98872643	0.275	6.36	
70.25	4303	3.75662268	1.06631582	0.284	6.85	
72.25	4444	3.82977089	1.10789568	0.289	7.15	
74.25	4584	3.58552214	1.03194635	0.288	7.07	
76.25	4724	3.65782247	1.02933251	0.281	6.72	

Depth (cm)	Calendar Age (yr BP)	Li/Ca	Mg/Ca	Mg/Li (mol $mmol^{-1}$)	Mg/Li T (°C)	Flagged Outlier
78.25	4865	3.87840401	1.0510211	0.271	6.15	
84.25	5286	3.88933267	1.06081661	0.273	6.25	
86.25	5426	3.62038732	1.2164851	0.336	9.82	1
88.25	5566	3.85927097	1.07121149	0.278	6.51	
90.25	5707	4.01745791	1.13885846	0.283	6.83	
92.25	5847	3.92496784	1.13674358	0.290	7.17	
94.25	5987	3.71667412	1.09483411	0.295	7.45	
96.25	6128	3.54824656	0.98553241	0.278	6.52	
98.25	6268	3.82672479	1.11789333	0.292	7.31	
100.25	6408	4.00599767	1.07835805	0.269	6.05	
103.25	6619	3.71358209	1.04818585	0.282	6.77	
106.25	6829	3.92142242	1.10602574	0.282	6.75	
110.25	7110	3.94075155	1.10222882	0.280	6.63	
114.25	7333	4.69105418	1.21860817	0.260	5.55	
116.25	7415	3.68191269	1.02857301	0.279	6.61	
120.25	7580	3.91290185	1.15307455	0.295	7.45	
122.25	7663	3.85562114	1.10445868	0.286	7.00	
124.25	7745	3.96134317	1.1013732	0.278	6.53	
126.25	7828	3.79531585	1.04251588	0.275	6.35	
128.25	7910	3.81030051	1.10246506	0.289	7.16	
130.25	7993	4.24393637	1.20896759	0.285	6.91	
132.25	8075	3.75826572	1.02323784	0.272	6.22	
134.25	8158	4.19283727	1.17245879	0.280	6.62	
136.25	8240	4.46296647	1.30128361	0.292	7.28	
138.25	8323	3.95698864	1.06770298	0.270	6.09	
140.25	8405	3.9629101	1.08123224	0.273	6.25	
142.25	8488	3.76629937	1.04938997	0.279	6.57	
144.25	8570	3.99521824	1.09078463	0.273	6.26	
146.25	8621	3.96368546	1.09918369	0.277	6.50	
148.25	8673	4.14192956	1.19217677	0.288	7.07	
150.25	8724	4.17874811	1.1444189	0.274	6.31	
152.25	8775	3.58159363	0.94781502	0.265	5.81	
154.25	8826	4.01923439	1.11492096	0.277	6.50	
156.25	8878	3.81497627	1.03480468	0.271	6.17	
158.25	8929	4.19353646	1.22869197	0.293	7.36	
160.25	8980	3.6479812	1.04130579	0.285	6.94	
162.25	9032	3.8662727	1.17321363	0.303	7.95	

Depth (cm)	Calendar Age (yr BP)	Li/Ca	Mg/Ca	Mg/Li (mol $mmol^{-1}$)	Mg/Li T (°C)	Flagged Outlier
164.25	9083	4.00984954	1.16102578	0.290	7.17	
166.25	9134	3.9429731	1.09869577	0.279	6.57	
168.25	9185	3.99709661	1.11835526	0.280	6.63	
170.25	9237	4.06940266	1.14384402	0.281	6.70	
172.25	9288	3.9733894	1.15645295	0.291	7.25	
174.25	9339	3.982784	1.10751136	0.278	6.54	
176.25	9390	4.54411693	1.30940702	0.288	7.09	
178.25	9442	4.05184722	1.13902437	0.281	6.70	
180.25	9493	4.14965375	1.21046348	0.292	7.29	
182.25	9544	4.58041886	1.34164849	0.293	7.36	
184.25	9596	4.06469028	1.26329768	0.311	8.36	
186.25	9647	4.10511019	1.1836622	0.288	7.10	
188.25	9698	3.83033755	1.11212862	0.290	7.21	
190.25	9749	4.15894069	1.22119831	0.294	7.40	
192.25	9801	3.97669448	1.1518261	0.290	7.17	
194.25	9852	4.82704211	1.45761228	0.302	7.86	
196.25	9903	4.14485713	1.20880931	0.292	7.28	
198.25	9955	4.35134914	1.26175852	0.290	7.19	
202.25	10057	4.62449133	1.36725415	0.296	7.51	
204.25	10108	3.72027802	1.10433181	0.297	7.57	
206.25	10160	4.00286466	1.16475636	0.291	7.25	
208.25	10211	4.11140538	1.1837041	0.288	7.08	
210.25	10262	4.14242056	1.17725767	0.284	6.87	
212.25	10313	4.01692473	1.17619083	0.293	7.35	
214.25	10365	4.5861697	1.3213148	0.288	7.09	
216.25	10416	4.7522891	1.32895665	0.280	6.62	
218.25	10438	4.18015617	1.22401541	0.293	7.35	
220.25	10459	3.88465745	1.1357249	0.292	7.33	
222.25	10481	4.87329129	1.31579028	0.270	6.10	
224.25	10503	3.97695913	1.14390737	0.288	7.06	
226.25	10524	4.122603	1.17720047	0.286	6.95	
228.25	10546	4.05706211	1.174755	0.290	7.17	
230.25	10568	3.86079548	1.13169853	0.293	7.37	
234.25	10611	4.45226771	1.27144901	0.286	6.95	
236.25	10633	4.15005515	1.19639095	0.288	7.10	
238.25	10655	3.89702615	1.12589236	0.289	7.13	
242.25	10698	4.65727299	1.40497309	0.302	7.85	

Depth (cm)	Calendar Age (yr BP)	Li/Ca	Mg/Ca	Mg/Li (mol $mmol^{-1}$)	Mg/Li T (°C)	Flagged Outlier
244.25	10720	4.35543447	1.28751347	0.296	7.51	
246.25	10741	4.06021916	1.25908497	0.310	8.32	
248.25	10763	3.68127969	1.37376553	0.373	12.07	1
250.25	10785	3.55738876	1.30221072	0.366	11.63	
252.25	10806	3.7490105	1.28351921	0.342	10.20	
254.25	10828	3.89956429	1.26130602	0.323	9.09	
256.25	10850	4.00139711	1.24773299	0.312	8.42	
258.25	10871	3.84882334	1.23780326	0.322	8.98	
260.25	10893	4.37217922	1.26735296	0.290	7.19	
262.25	10915	4.84621062	1.39469307	0.288	7.07	
264.25	10937	4.24298542	1.27030627	0.299	7.72	
266.25	10958	4.36914964	1.31273548	0.300	7.78	
268.25	10980	4.26313859	1.25949071	0.295	7.50	
270.25	11002	3.83437444	1.1393115	0.297	7.59	
272.25	11023	4.2529863	1.32955923	0.313	8.47	
274.25	11045	3.86100203	1.128378	0.292	7.32	
276.25	11067	4.30383003	1.2479066	0.290	7.19	
278.25	11088	4.32020324	1.41869223	0.328	9.38	
280.25	11110	4.22705876	1.2461458	0.295	7.46	
282.25	11122	4.32252438	1.29277278	0.299	7.70	
284.25	11134	3.89597443	1.12202473	0.288	7.08	
286.25	11147	4.2236633	1.23186495	0.292	7.29	
288.25	11159	4.21146603	1.22316191	0.290	7.22	
290.25	11171	4.01418482	1.21913995	0.304	7.96	
292.25	11183	4.01418888	1.16480468	0.290	7.20	
294.25	11196	4.36329961	1.27917048	0.293	7.37	
298.25	11220	4.12645674	1.2610056	0.306	8.07	
302.25	11244	3.91227445	1.21672484	0.311	8.37	
304.25	11257	4.0947546	1.2309962	0.301	7.79	
306.25	11269	4.36492103	1.29474121	0.297	7.56	
308.25	11281	4.31146447	1.26493298	0.293	7.38	
310.25	11293	4.33914276	1.30272341	0.300	7.76	
312.25	11306	4.15994062	1.17844612	0.283	6.82	
314.25	11318	4.08734202	1.14169631	0.279	6.61	
316.25	11330	4.20220641	1.25108585	0.298	7.62	
319.25	11348	4.2822316	1.24338758	0.290	7.21	
324.25	11379	4.06754661	1.18601901	0.292	7.28	

Depth (cm)	Calendar Age (yr BP)	Li/Ca	Mg/Ca	Mg/Li (mol $mmol^{-1}$)	Mg/Li T (°C)	Flagged Outlier
326.25	11391	4.35567851	1.2815025	0.294	7.43	
328.25	11403	3.97126707	1.18216262	0.298	7.62	
330.25	11416	4.25161245	1.23679462	0.291	7.24	
332.25	11428	4.19815837	1.1895365	0.283	6.83	
334.25	11440	4.20556814	1.22917791	0.292	7.32	
336.25	11452	3.90625014	1.15426575	0.295	7.50	
340.25	11477	3.95903217	1.18074472	0.298	7.65	
430.25	12027	3.66729897	1.19761787	0.327	9.27	
440.25	12088	4.10610628	1.56061619	0.380	12.50	1
448.25	12149	4.16424145	1.34926283	0.324	9.12	
454.25	12198	5.24869136	1.97075117	0.375	12.22	1
456.25	12215	4.28956126	1.38067139	0.322	9.00	
458.25	12231	4.04658197	1.31922354	0.326	9.24	
462.25	12264	3.82957212	1.2219133	0.319	8.84	
464.25	12280	4.37966458	1.35137622	0.309	8.24	
466.25	12287	5.09580836	1.41106861	0.277	6.47	
468.25	12294	4.19530131	1.39987512	0.334	9.69	
472.25	12307	3.89685638	1.20811968	0.310	8.32	
474.25	12314	4.49500408	1.45825709	0.324	9.15	
476.25	12321	4.02364133	1.26339056	0.314	8.55	
478.25	12327	4.4441201	1.37668331	0.310	8.30	
480.25	12334	4.16761714	1.31762726	0.316	8.67	
484.25	12348	4.11164312	1.31280087	0.319	8.85	
486.25	12354	3.78950265	1.22650297	0.324	9.10	
488.25	12361	4.27660191	1.31040551	0.306	8.11	
492.25	12375	4.18911553	1.30542893	0.312	8.41	
496.25	12388	4.44198484	1.35822165	0.306	8.08	
498.25	12395	4.20063753	1.33468447	0.318	8.76	
500.25	12402	3.83530597	1.19685358	0.312	8.44	
504.25	12415	4.6923219	1.50118689	0.320	8.89	
506.25	12422	4.60280948	1.45792865	0.317	8.70	
508.25	12429	5.09467386	1.64106579	0.322	9.01	
512.25	12442	4.17026722	1.33703374	0.321	8.93	
514.25	12449	3.83014227	1.20909712	0.316	8.64	
516.25	12456	4.83774894	1.48972594	0.308	8.20	
518.25	12462	5.00171131	1.52492451	0.305	8.03	
520.25	12469	5.39297639	1.39587703	0.259	5.50	

Depth (cm)	Calendar Age (yr BP)	Li/Ca	Mg/Ca	Mg/Li (mol $mmol^{-1}$)	Mg/Li T (°C)	Flagged Outlier
524.25	12483	4.77981224	1.38208997	0.289	7.15	
542.25	12543	3.7863286	1.15834835	0.306	8.09	
548.25	12576	4.14677801	1.31340912	0.317	8.70	
552.25	12602	4.64453728	1.39880701	0.301	7.82	
556.25	12628	4.43275096	1.37865256	0.311	8.38	
558.25	12640	4.26636623	1.1586787	0.272	6.18	
562.25	12666	5.13215121	1.63526827	0.319	8.81	
564.25	12679	4.47390649	1.39239132	0.311	8.39	
566.25	12692	4.43498827	1.43213239	0.323	9.06	
568.25	12705	4.26779149	1.46666377	0.344	10.28	
570.25	12718	4.18356711	1.32543663	0.317	8.71	
572.25	12731	3.86829727	1.22080352	0.316	8.64	
574.25	12744	4.17239327	1.34219401	0.322	8.99	
576.25	12757	4.48058516	1.42639132	0.318	8.80	
578.25	12770	4.03198049	1.25807219	0.312	8.43	
580.25	12783	4.22217965	1.353711	0.321	8.93	
582.25	12795	3.99659922	1.24408096	0.311	8.39	
584.25	12808	3.98338253	1.24047386	0.311	8.40	
586.25	12821	4.22055488	1.28199412	0.304	7.96	
588.25	12834	3.98594949	1.26802224	0.318	8.78	
590.25	12847	3.58819988	1.19479575	0.333	9.65	
594.25	12893	4.129344	1.28543954	0.311	8.39	
598.25	12959	3.96561098	1.23759201	0.312	8.44	
604.25	13058	4.49752608	1.2915076	0.287	7.04	
606.25	13091	4.36725238	1.30476761	0.299	7.68	
612.25	13197	4.73280767	1.35386204	0.286	6.98	
614.25	13232	3.93868945	1.14509749	0.291	7.23	
616.25	13267	4.08920071	1.19434104	0.292	7.31	
624.25	13408	4.77638087	1.33959766	0.280	6.67	
626.25	13443	4.18282443	1.1243639	0.269	6.03	
630.25	13513	4.22426866	1.18833803	0.281	6.71	
636.25	13619	5.87800535	1.74947974	0.298	7.62	
638.25	13654	4.17250645	1.16772678	0.280	6.63	
644.25	13760	4.0831197	1.13191061	0.277	6.49	
648.25	13830	4.32853291	1.30642574	0.302	7.85	
652.25	13964	3.99734659	1.08124307	0.270	6.12	
654.25	14031	4.34980431	1.21453633	0.279	6.60	

Depth (cm)	Calendar Age (yr BP)	Li/Ca	Mg/Ca	Mg/Li (mol $mmol^{-1}$)	Mg/Li T (°C)	Flagged Outlier
660.25	14233	4.25124696	1.15760098	0.272	6.22	
662.25	14300	4.37128794	1.23159988	0.282	6.74	
664.25	14367	3.97650912	1.10545927	0.278	6.53	
666.25	14434	4.16862394	1.16857749	0.280	6.66	
668.25	14501	4.26482532	1.23735985	0.290	7.20	
670.25	14569	4.28971243	1.20635258	0.281	6.71	
672.25	14636	3.83937801	1.11972724	0.292	7.29	
674.25	14703	4.25487133	1.19493347	0.281	6.69	
676.25	14770	4.0449189	1.17193302	0.290	7.18	
678.25	14837	4.62270742	1.34409339	0.291	7.24	
680.25	14904	4.03589618	1.15853194	0.287	7.03	
682.25	14971	4.23297492	1.26192815	0.298	7.65	
684.25	15039	7.60985984	1.91106011	0.251	5.09	
688.25	15173	4.20811295	1.20804119	0.287	7.03	
690.25	15240	4.4841744	1.29307251	0.288	7.10	
692.25	15307	4.69731668	1.3970895	0.297	7.61	
694.25	15374	5.80405226	1.51997199	0.262	5.66	
696.25	15441	4.76992477	1.3217096	0.277	6.48	
700.25	15576	5.08253744	1.61563666	0.318	8.77	
702.25	15643	4.60468253	1.23696464	0.269	6.02	
704.25	15710	4.19563623	1.21046906	0.289	7.11	
708.25	16006	4.80088671	1.36963186	0.285	6.93	
710.25	16154	4.89808288	1.59162456	0.325	9.18	
712.25	16301	5.69343759	1.67829072	0.295	7.46	
730.25	17632	5.18608972	1.38842135	0.268	5.97	
734.25	17843	5.81566686	1.25539786	0.216	3.25	
738.25	17969	6.75336151	1.51279428	0.224	3.67	
740.25	18032	6.38285412	1.33819483	0.210	2.94	
746.25	18221	6.65000825	1.39407937	0.210	2.94	
758.25	18711	6.00382753	1.25659959	0.209	2.92	
760.25	18812	7.33030606	1.5246415	0.208	2.85	
764.25	19012	5.643436135	1.689228378	0.299	7.71	1
778.25	19715	6.56671441	1.3756622	0.209	2.93	
804.25	21051	6.313452	1.373693593	0.218	3.34	
806.25	21183	6.67929939	1.39589745	0.209	2.90	
808.25	21314	5.792998545	2.231816009	0.385	12.83	1
812.25	21577	6.4597498	1.39281783	0.216	3.24	

Depth (cm)	Calendar Age (yr BP)	Li/Ca	Mg/Ca	Mg/Li (mol mmol^{-1})	Mg/Li T (°C)	Flagged Outlier
814.25	21708	6.0926315	1.34526677	0.221	3.51	
818.25	21970	6.21781189	1.35521447	0.218	3.36	
822.25	22233	5.893154617	1.295030459	0.220	3.45	
828.25	22627	5.349342519	1.353581529	0.253	5.19	
830.25	22758	5.65840644	1.31546795	0.232	4.11	
834.25	23021	5.60920244	1.59513166	0.284	6.88	
836.25	23152	4.41865427	1.21795205	0.276	6.40	
838.25	23283	7.29399455	1.6207977	0.222	3.58	
842.25	23546	5.45734681	1.20528898	0.221	3.51	
844.25	23677	5.56178936	1.2781471	0.230	3.97	
846.25	23809	6.01476681	1.45087825	0.241	4.56	
848.25	23940	5.254491366	1.19105369	0.227	3.81	
850.25	24026	5.4741462	1.32683696	0.242	4.59	
854.25	24198	5.82404327	1.57653679	0.266	5.90	
856.25	24284	6.110038785	1.367754598	0.224	3.66	
858.25	24370	5.17355137	1.15751719	0.224	3.65	
860.25	24456	5.608619896	1.25226234	0.223	3.63	
862.25	24542	5.70700374	1.65158815	0.290	7.17	1
864.25	24628	5.431881537	1.359964724	0.250	5.05	
866.25	24714	5.61554318	1.25348238	0.224	3.65	
868.25	24800	7.849801058	1.809509144	0.231	4.01	
870.25	24886	5.91299955	1.4335185	0.239	4.47	
874.25	25058	5.319497065	1.266385334	0.238	4.40	
876.25	25144	6.298180664	1.316275191	0.209	2.90	
878.25	25230	5.837942629	1.256333766	0.215	3.22	
886.25	25761	5.921728503	1.274332731	0.215	3.22	
888.25	25894	5.39380695	1.25746303	0.233	4.14	
892.25	26159	5.60942775	1.23423412	0.220	3.47	
894.25	26292	5.37122315	1.07960685	0.201	2.50	
896.25	26424	5.61965293	1.1951018	0.213	3.09	
898.25	26557	5.28966634	1.10017956	0.208	2.85	
900.25	26690	5.7507178	1.14538929	0.199	2.41	
902.25	26822	5.74076758	1.24664867	0.217	3.32	
904.25	26955	5.58250404	1.20165368	0.215	3.22	
906.25	27088	5.18551209	1.12772245	0.218	3.35	
908.25	27221	4.94482293	1.07576262	0.218	3.34	
910.25	27353	5.31845499	1.12852129	0.212	3.07	

Depth (cm)	Calendar Age (yr BP)	Li/Ca	Mg/Ca	Mg/Li (mol $mmol^{-1}$)	Mg/Li T (°C)	Flagged Outlier
912.25	27486	5.35773194	1.10451687	0.206	2.76	
914.25	27619	5.72419178	1.36017816	0.238	4.38	
918.25	27884	5.13940792	1.14107178	0.222	3.57	
920.25	28017	5.62189547	1.27792024	0.227	3.84	
922.25	28149	5.51037261	1.19417577	0.217	3.30	
924.25	28282	5.70570815	1.29736106	0.227	3.84	
926.25	28415	5.73976405	1.31088537	0.228	3.90	
928.25	28548	5.80069294	1.30787061	0.225	3.75	
932.25	28813	6.02150673	1.31564241	0.218	3.39	
934.25	28946	5.19450793	1.19143488	0.229	3.95	
936.25	29078	6.0479653	1.43930975	0.238	4.39	
938.25	29211	5.24597626	1.23411146	0.235	4.25	
940.25	29344	5.70031159	1.27146896	0.223	3.62	
942.25	29476	5.32476052	1.17029878	0.220	3.45	
946.25	29742	6.63026645	1.26338342	0.191	1.98	
950.25	30007	6.00930274	1.23070406	0.205	2.69	
952.25	30140	5.192271	1.12757843	0.217	3.32	
954.25	30185	5.51998412	1.21246556	0.220	3.45	
956.25	30229	6.09178188	1.26885139	0.208	2.87	
958.25	30274	5.65685676	1.21438586	0.215	3.19	
960.25	30318	5.57750166	1.22764118	0.220	3.47	
962.25	30363	5.83070428	1.3985549	0.240	4.49	
964.25	30407	4.23472109	1.07472951	0.254	5.23	
966.25	30452	4.92984427	1.12653363	0.229	3.90	
968.25	30496	5.94542096	1.55738231	0.262	5.66	
970.25	30541	5.9460158	2.45346575	0.413	14.61	1
972.25	30585	5.58049123	1.17628606	0.211	2.99	
974.25	30630	6.06987116	1.34612674	0.222	3.55	
976.25	30674	5.76069733	1.21019002	0.210	2.96	
978.25	30719	5.32428523	1.34486265	0.253	5.16	
980.25	30763	5.24663561	1.18705109	0.226	3.79	
982.25	30808	6.04999525	1.24531127	0.206	2.74	
984.25	30852	5.73539683	1.28686224	0.224	3.69	
986.25	30897	5.29880327	1.10198478	0.208	2.85	
988.25	30941	5.81736286	1.26916217	0.218	3.37	
990.25	30986	5.61732356	1.22545622	0.218	3.37	
992.25	31030	5.72743558	1.2500004	0.218	3.37	

Depth (cm)	Calendar Age (yr BP)	Li/Ca	Mg/Ca	Mg/Li (mol $mmol^{-1}$)	Mg/Li T (°C)	Flagged Outlier
994.25	31075	5.6049961	1.71984606	0.304	8.00	1
996.25	31119	5.167970759	1.202809589	0.233	4.12	
998.25	31164	5.1280899	1.17500677	0.229	3.93	
1000.25	31208	4.89960991	1.1281191	0.230	3.99	
1002.25	31253	5.69480277	2.08468428	0.366	11.63	1
1004.25	31297	4.81219366	1.19076168	0.248	4.92	
1006.25	31342	4.28897936	1.0082382	0.235	4.24	
1008.25	31386	4.95693681	1.16367642	0.235	4.23	
1010.25	31431	5.05257994	1.18535054	0.235	4.22	
1012.25	31475	4.49511722	1.15012805	0.257	5.42	
1014.25	31520	4.7730631	1.13738748	0.238	4.41	
1016.25	31569	5.7580595	1.4110437	0.245	4.77	
1018.25	31618	4.81933482	1.13573995	0.236	4.27	
1020.25	31667	4.74633595	1.26648011	0.267	5.93	
1022.25	31716	3.58327868	1.10380217	0.308	8.21	1
1024.25	31765	4.73062477	1.12167781	0.237	4.35	
1026.25	31814	12.1022487	1.20786479	0.100	-2.35	1
1028.25	31863	5.0641013	1.19786273	0.237	4.32	
1030.25	31912	4.88146321	1.16143124	0.238	4.39	
1032.25	31961	4.86107517	1.17576486	0.242	4.60	
1034.25	32010	4.85539419	1.17595475	0.242	4.62	
1036.25	32059	4.56581565	1.72817597	0.379	12.41	1
1038.25	32108	4.85346444	1.19626677	0.246	4.84	
1040.25	32157	4.38481767	1.05848535	0.241	4.57	
1042.25	32206	4.661238316	1.093697915	0.235	4.22	
1044.25	32255	4.491668714	1.175859207	0.262	5.65	
1046.25	32304	4.573266314	1.040418262	0.228	3.85	
1048.25	32353	4.590332379	1.131221931	0.246	4.84	
1050.25	32402	4.452497788	1.126107628	0.253	5.18	
1052.25	32451	4.5308014	1.091917205	0.241	4.55	
1054.25	32500	4.674404805	1.076244467	0.230	3.99	
1056.25	32549	4.577512546	1.195115869	0.261	5.62	
1058.25	32598	4.242278406	0.96810616	0.228	3.89	
1060.25	32647	4.082688243	1.076219726	0.264	5.75	
1062.25	32696	4.448564482	1.170528378	0.263	5.73	
1064.25	32745	4.486546902	1.165756052	0.260	5.55	
1066.25	32794	4.453374506	1.150850443	0.258	5.47	

Depth (cm)	Calendar Age (yr BP)	Li/Ca	Mg/Ca	Mg/Li (mol $mmol^{-1}$)	Mg/Li T (°C)	Flagged Outlier
1068.25	32843	4.4198394	1.278471691	0.289	7.15	
1070.25	32892	4.833820333	1.194594502	0.247	4.87	
1072.25	32941	4.639058974	1.906459857	0.411	14.50	1
1074.25	32990	4.656453725	1.545819948	0.332	9.59	1
1076.25	33072	4.670228258	1.211565517	0.259	5.53	
1078.25	33154	4.426971187	1.214717724	0.274	6.34	
1080.25	33236	4.442247559	1.165201788	0.262	5.68	
1084.25	33400	4.201592004	1.197993382	0.285	6.92	
1086.25	33482	4.305942882	1.153676073	0.268	5.99	
1088.25	33564	4.324598128	1.253651618	0.290	7.19	
1090.25	33646	4.455837315	1.163010751	0.261	5.61	
1092.25	33728	4.67170167	1.20929888	0.259	5.50	
1094.25	33810	4.411323381	1.133624155	0.257	5.40	
1096.25	33892	4.449774662	1.134466031	0.255	5.29	
1098.25	33974	4.103475874	1.081305954	0.264	5.75	
1100.25	34056	4.611083008	1.275428664	0.277	6.46	
1102.25	34138	4.273034648	1.077133671	0.252	5.14	
1104.25	34220	3.969377137	1.032452129	0.260	5.56	
1106.25	34254	4.212662458	1.103636574	0.262	5.67	
1108.25	34289	4.562875568	1.216727562	0.267	5.92	
1110.25	34323	4.287936814	1.127174575	0.263	5.71	
1112.25	34357	4.098279817	1.079265145	0.263	5.74	
1116.25	34426	3.926029902	1.058064798	0.269	6.07	
1118.25	34460	4.089963602	1.210331303	0.296	7.52	
1120.25	34494	4.569148025	1.267677557	0.277	6.50	

APPENDIX C. SUPPLEMENTARY FIGURE 2-1: COMPARISON OF MG/LI AND LI/MG-DERIVED TEMPERATURES

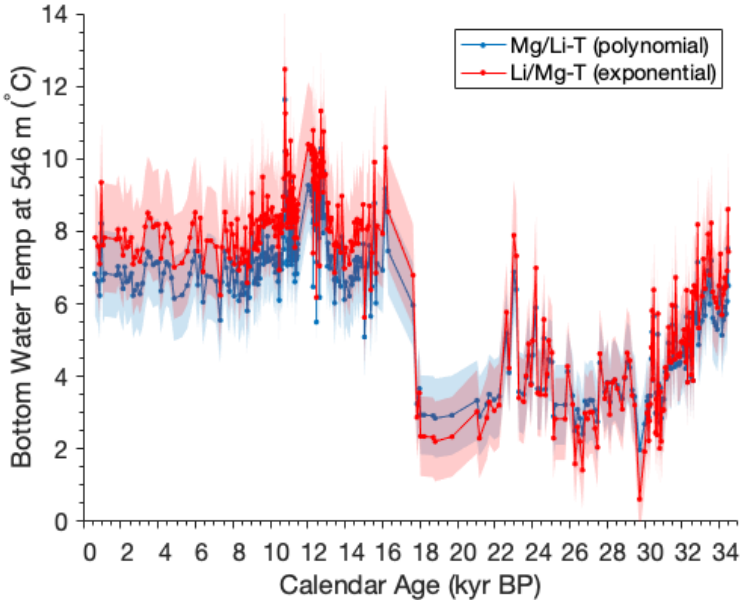

Supplementary Figure 2-1. Comparison of Mg/Li and Li/Mg-derived temperatures, from *Valley et al.*, 2019- intermediate depth water temperature with error ranges (1s).

Mg/Li derived temperature equation:
$Mg/Li = 0.150 \pm 0.012 + 0.0209 \pm 0.0027T - 0.0002 \pm 0.0001\ T^2$
Marchitto et al., 2018 equation 5

Li/Mg derived temperature equation:
$Li/Mg = 5.43 \pm 0.11e^{-0.0551 \pm 0.0024T}$
Marchitto et al., 2018 equation 1

APPENDIX D. FLORIDA STRAITS COMMON ERA RECORDS CORE INFORMATION AND CD_W

Quality code 1 indicates potentially contaminated samples removed from analysis. Outliers beyond 2 standard deviations of a Lowess smoothed time series are indicated as 1 and omitted from interpretation.

Core	Water Depth	Latitude	Longitude
KNR 166-2 3MC-H	447 m	24 23.04 N	83 20.33 W

Core depth (cm)	Calendar Age (yr BP)	Cdw	Quality Code	Flagged as Outlier
1	0	0.384		
3.5	76	0.415		
5.5	136	0.396		
6.5	167	0.360		1
7.5	197	0.349		
9.5	257	0.298		
10.5	288	0.384		1
11.5	318	0.317		
13.5	379	0.396		
14.5	409	0.388		
18.5	530	0.393		1
19.5	561	0.378		
21.5	622	0.287		
37.5	1110	0.346		

Core	Water Depth	Latitude	Longitude
KNR 166-2 62MCA	547 m	24 19.60 N	83 15.40 W

Core depth (cm)	Calendar Age (yr BP)	Cdw	Quality Code	Flagged as Outlier
0.25	0	0.261		1
1.25	38	0.390		
1.75	64	0.404		
2.25	89	0.376		
2.75	115	0.358		
3.25	140	0.567		
3.75	166	0.339		
4.75	216	0.377		
5.25	242	0.352		
5.75	267	0.332		1
6.25	293	0.382		
6.75	318	0.432		
7.25	344	0.397		
7.75	369	0.366		
8.25	395	0.427		
8.75	420	0.393		
9.25	446	0.363		
9.75	471	0.397		
10.25	497	0.424		
10.75	522	0.422		
11.75	546	0.421		
12.25	558	0.318		
12.75	570	0.344		
13.25	582	0.427		
13.75	594	0.434		
14.25	606	0.413		
14.75	618	0.438		
15.25	630	0.431		
15.75	642	0.335		
16.25	654	0.366		

Core depth (cm)	Calendar Age (yr BP)	Cdw	Quality Code	Flagged as Outlier
16.75	666	0.420		
17.25	678	0.398		
17.75	690	0.377		
18.25	702	0.381		
18.75	714	0.339		
19.25	726	0.385		
19.75	738	0.369		1
20.25	750	0.428		
20.75	762	0.357		
21.25	774	0.376		
21.75	786	0.358		
22.25	798	0.350		
22.75	810	0.324		
23.25	822	0.467		
23.75	834	0.362		
24.25	846	0.375		
24.75	858	0.390		
25.25	870	0.355		
25.75	882	0.384		
26.25	894	0.374		
26.75	906	0.371		
27.25	918	0.408		
27.75	930	0.411		
28.25	942	0.429		
28.75	954	0.395		
29.25	966	0.372		
29.75	978	0.379		

Core	Water Depth	Latitude	Longitude
W167-79GCC	530 m	24 21.50 N	83 20.90 W

Core depth (cm)	Calendar Age (yr BP)	Cdw	Quality Code	Flagged as Outlier
2	109	0.320		
3.25	200	0.346		
3.75	236	0.430		
4.25	273	0.308		
5.25	346	0.454		
5.75	382	0.343		
6.25	418	0.374		1
6.75	455	0.342		
7.25	491	0.527		
7.75	527	0.506		
8.25	564	0.451		
9.25	597	0.358		
9.75	606	0.361		
10.25	616	0.374		1
10.75	626	0.384		
11.25	636	0.359		
11.75	646	0.433		
12.25	655	0.535		
12.75	665	0.410		
13.25	675	0.534		
13.75	685	0.421		
14.25	695	0.559		
14.75	704	0.347		
15.75	724	0.404		
16.25	734	0.430		
16.75	744	0.371		
17.25	753	0.598		
17.75	763	0.439		
18.25	773	0.340		

Core depth (cm)	Calendar Age (yr BP)	Cdw	Quality Code	Flagged as Outlier
18.75	783	0.383		
19.25	793	0.511		
19.75	802	0.380		
20.25	812	0.479		
20.75	828	0.371		
21.25	850	0.416		
21.75	871	0.375		
22.25	893	0.405		
22.75	915	0.466		

APPENDIX E. FLORIDA STRAITS COMMON ERA RECORDS CORE INFORMATION, MG/LI AND MG/LI-DERIVED TEMPERATURES

Quality code 1 indicates potentially contaminated samples removed from analysis. Outliers beyond 2 standard deviations of a Lowess smoothed time series are indicated as 1 and omitted from interpretation.

Core	Water Depth	Latitude	Longitude
KNR 166-2 3MC-H	447 m	24 23.04 N	83 20.33 W

Core depth (cm)	Calendar Age (yr BP)	Mg/Li (mol $mmol^{-1}$)	Mg/Li T (°C)	Quality Code	Flagged as Outlier
1	0	0.28332284	6.82		
3.5	76	0.2902685	7.21		
5.5	136	0.29537517	7.49		
6.5	167	0.29721296	7.60		
7.5	197	0.28465016	6.90		
9.5	257	0.29059264	7.23		
10.5	288	0.27617109	6.43		
11.5	318	0.28819651	7.09		
13.5	379	0.30845459	8.23		
14.5	409	0.29373951	7.40		
18.5	530	0.28686058	7.02		
19.5	561	0.29891436	7.69		
21.5	622	0.35441156	10.92		1
37.5	1110	0.29803007	7.64		

Core	Water Depth	Latitude	Longitude
KNR 166-2 62MCA	547 m	24 19.60 N	83 15.40 W

Core depth (cm)	Calendar Age (yr BP)	Mg/Li (mol $mmol^{-1}$)	Mg/Li T (°C)	Quality Code	Flagged as Outlier
0.25	0	0.19396119	n/a	1	
1.25	38	0.03127993	n/a	1	
1.75	64	0.18481435	n/a	1	
2.25	89	0.27810598	6.54		
2.75	115	0.28124887	6.71		
3.25	140	0.26461416	5.81		
3.75	166	0.24114087	n/a	1	
4.75	216	0.27778087	6.52		
5.25	242	4.4082813	n/a	1	
5.75	267	0.41154468	n/a	1	
6.25	293	0.25621066	n/a	1	
6.75	318	0.44613775	n/a	1	
7.25	344	0.28034343	6.66		
7.75	369	0.43364193	16.03	1	
8.25	395	0.30001724	7.75		
8.75	420	0.72282307	n/a	1	
9.25	446	0.61267819	n/a	1	
9.75	471	0.36832889	11.77		1
10.25	497	0.27009428	6.10		
10.75	522	0.27038763	6.12		
11.75	546	0.29679887	7.57		
12.25	558	0.27931176	6.60		
12.75	570	0.28852156	7.11		
13.25	582	0.2751147	6.38		
13.75	594	0.27252048	6.23		
14.25	606	0.2709078	6.15		
14.75	618	0.28180595	6.74		
15.25	630	0.29232985	7.32		
15.75	642	0.28670635	7.01		

Core depth (cm)	Calendar Age (yr BP)	Mg/Li (mol $mmol^{-1}$)	Mg/Li T (°C)	Quality Code	Flagged as Outlier
16.25	654	0.26441264	5.80		
16.75	666	0.29654243	7.56		
17.25	678	0.27398552	6.31		
17.75	690	0.26852713	6.02		
18.25	702	0.27672738	6.46		
18.75	714	0.26962589	6.08		
19.25	726	0.27405213	6.32		
19.75	738	0.2705867	6.13		
20.25	750	0.27850702	6.56		
20.75	762	0.27906105	6.59		
21.25	774	0.27051321	6.13		
21.75	786	0.26068632	5.60		
22.25	798	0.26769804	5.97		
22.75	810	0.27766125	6.51		
23.25	822	0.27245585	6.23		
23.75	834	0.26033921	5.58		
24.25	846	0.26630815	5.90		
24.75	858	0.26137198	5.63		
25.25	870	0.27235399	6.23		
25.75	882	0.27125668	6.17		
26.25	894	0.27641429	6.45		
26.75	906	0.27236855	6.23		
27.25	918	0.27081037	6.14		
27.75	930	0.27312699	6.27		
28.25	942	0.26264966	5.70		
28.75	954	0.26304606	5.72		
29.25	966	0.27399172	6.31		
29.75	978	0.26649529	5.91		

Core	Water Depth	Latitude	Longitude
W167-79GGC	530 m	24 21.50 N	83 20.90 W

Core depth (cm)	Calendar Age (yr BP)	Mg/Li (mol $mmol^{-1}$)	Mg/Li T (°C)	Quality Code	Flagged as Outlier
2	109	0.27830681	6.55		
3.25	200	0.27619462	6.43		
3.75	236	0.29819674	7.65		
4.25	273	0.2800535	6.65		
5.25	346	0.29733343	7.60		
5.75	382	0.27923668	6.60		
6.25	418	0.26893496	6.04		
6.75	455	0.28409644	6.87		
7.25	491	0.29735533	7.60		
7.75	527	0.25472358	5.28		
8.25	564	0.28895935	7.14		
9.25	597	0.28308308	6.81		
9.75	606	0.27730477	6.49		
10.25	616	0.28297802	6.81		
10.75	626	0.3073556	8.17		
11.25	636	0.27378603	6.30		
11.75	646	0.27791681	6.53		
12.25	655	0.27373751	6.30		
12.75	665	0.27128685	6.17		
13.25	675	0.27798033	6.53		
13.75	685	0.26335104	5.74		
14.25	695	0.26531497	5.84		
14.75	704	0.27611269	6.43		
15.75	724	0.28349432	6.83		
16.25	734	0.33690538	9.88		1
16.75	744	0.293359	7.38		
17.25	753	0.22647278	3.80		1
17.75	763	0.27775164	6.52		
18.25	773	0.30617168	8.10		

Core depth (cm)	Calendar Age (yr BP)	Mg/Li (mol $mmol^{-1}$)	Mg/Li T (°C)	Quality Code	Flagged as Outlier
18.75	783	0.28009412	6.65		
19.25	793	0.270326	6.12		
19.75	802	0.28453262	6.89		
20.25	812	0.28186342	6.74		
20.75	828	0.27674096	6.46		
21.25	850	0.28091978	6.69		
21.75	871	0.28906829	7.14		
22.25	893	0.27284952	6.25		
22.75	915	0.28338212	6.83		

REFERENCES

Adkins, J.F., Schrag, D.P., (2001). Pore fluid constraints on deep ocean temperature and salinity during the Last Glacial Maximum. Geophys. Res. Lett. 28 (5), 771–774. https://doi.org/10.1029/2000GL011597.

Adkins, J. F. (2013). The role of deep ocean circulation in setting glacial climates. Paleoceanography, 28, 539–561. https://doi.org/10.1002/ palo.20046

Andersen, K. K., Azuma, N., Barnola, J.-M., Bigler, M., Biscaye, P., Caillon, N., ... White, J. W. C. (2004). High-resolution record of Northern Hemisphere climate extending into the last interglacial period. Nature, 431(7005), 147–151. https://doi.org/10.1038/nature02805

Andersen, K.K., Svensson, A., Johnsen, S.J., Rasmussen, S.O., Bigler, M., Röthlisberger, R., Ruth, U., Siggaard-Andersen, M.-L., Steffensen, J.P., Dahl-Jensen, D., (2006). The Greenland Ice Core Chronology 2005, 15–42 ka. Part 1: constructing the time scale. Quat. Sci. Rev. 25 (23–24), 3246–3257. https://doi.org/10.1016/j.quascirev. 2006.08.002.

Bingham, R.J., Hughes, C.W., Roussenov, V., Williams, R.G., (2007). Meridional coherence of the North Atlantic meridional overturning circulation. Geophysical Research Letters 34, n/a–n/a. doi:10.1029/2007GL031731

Bond, G., Broecker, W., Johnsen, S., McManus, J., Labeyrie, L., Jouzel, J., & Bonani, G. (1993). Correlations between climate records from North Atlantic sediments and Greenland ice. Nature, 365(6442), 143–147. https://doi.org/10.1038/365143a0

Boyle, E. A., Sclater, F., & Edmond, J. M. (1976). On the marine geochemistry of cadmium. Nature, 263(5572), 42–44. https://doi.org/10.1038/ 263042a0

Boyle, E. A., & Keigwin, L. D. (1985). Comparison of Atlantic and Pacific paleochemical records for the last 215,000 years: Changes in deep ocean circulation and chemical inventories. Paleoceanography, 76(1–2), 135–150. https://doi.org/10.1016/0012-821x(85)90154-2

Boyle, E. A., & Keigwin, L. (1987). North Atlantic thermohaline circulation during the past 20,000 years linked to high-latitude surface temperature. Nature, 330(6143), 35–40. https://doi.org/10.1038/330035a0

Boyle, E. (1992). Cadmium and delta-13-C paleochemical ocean distributions during the Stage 2 Glacial Maximum. Annual Review of Earth and Planetary Sciences, 20(1), 245–287. https://doi.org/10.1146/annurev.earth.20.1.245

Boyle, E. A., Labeyrie, L., & Duplessly, J.-C. (1995). Calcitic foraminiferal data confirmed by cadmium in aragonitic Hoeglundina: Application to the last glacial maximum in the northern Indian Ocean. Paleoceanography, 10(5), 881–900. https://doi.org/10.1029/ 95PA01625

Boyle, E., & Rosenthal, Y. (1996). Chemical hydrography of the South Atlantic during the Last Glacial Maximum: Cd vs. δ13C. In the South Atlantic (pp. 423–443). Berlin: Springer. https://doi.org/10.1007/978-3-642-80353-6_23

Bradtmiller, L. I., McManus, J. F., & Robinson, L. F. (2014). $^{231}Pa/^{230}$ Th evidence for a weakened but persistent Atlantic meridional overturning circulation during Heinrich Stadial 1. Nature Communications, 5, 5817. https://doi.org/10.1038/ncomms6817

Broecker, W. S., & Maier Reimer, E. (1992). The influence of air and sea exchange on the carbon isotope distribution in the sea. Global Biogeochemical Cycles, 6(3), 315–320. https://doi.org/10.1029/92GB01672

Broecker, W. S. (1994). Massive iceberg discharges as triggers for global climate change. Nature, 372(6505), 421–424. https://doi.org/10.1038/ 372421a0

Broecker, W.S., (1998). Paleocean circulation during the Last Deglaciation: A bipolar seesaw? paleoceanography 13, 119–121. doi:10.1029/97PA03707

Bryan, S.P., Marchitto, T.M., (2008). Mg/Ca-temperature proxy in benthic foraminifera: new calibrations from the Florida Straits and a hypothesis regarding Mg/Li. Paleoceanography 23 (2). https://doi.org/10.1029/2007pa001553.

Bryan, S. P., & Marchitto, T. M. (2010). Testing the utility of paleonutrient proxies Cd/Ca and Zn/Ca in benthic foraminifera from thermocline waters. Geochemistry, Geophysics, Geosystems, 11(1), Q01005. https://doi.org/10.1029/2009GC002780

Buckley, M.W., Ferreira, D., Campin, J., Marshall, J., Tulloch, R., Buckley, M.W., Ferreira, D., Campin, J.-M., Marshall, J., Tulloch, R., (2012). On the relationship between decadal buoyancy anomalies and variability of the Atlantic meridional overturning circulation. BAMS. doi:10.1175/JCLI-D-11-00505.1

Butzin, M., Prange, M., & Lohmann, G. (2012). Readjustment of glacial radiocarbon chronologies by self-consistent three-dimensional ocean circulation modeling. Earth and Planetary Science Letters, 317-318, 177–184. https://doi.org/10.1016/j.epsl.2011.11.046

Came, R.E., Curry, W.B., Oppo, D.W., Broccoli, A.J., Stouffer, R.J., Lynch-Stieglitz, J., (2007). North Atlantic intermediate depth variability during the Younger Dryas: evidence from benthic foraminiferal Mg/Ca and the GFDL R30 Coupled Climate Model. In: Millennial-Scale Interhemispheric Asymmetry of Low-Latitude Pre-

cipitation: Speleothem Evidence and Possible High-Latitude Forcing, vol. 173. American Geophysical Union, Washington D.C., pp. 247–263.

Came, R. E., Oppo, D. W., Curry, W. B., & Lynch-Stieglitz, J. (2008). Deglacial variability in the surface return flow of the Atlantic meridional overturning circulation. Paleoceanography, 23, PA1217. https://doi.org/10.1029/2007PA001450

Case, D.H., Robinson, L.F., Auro, M.E., Gagnon, A.C., (2010). Environmental and biological controls on Mg and Li in deep-sea scleractinian corals. Paleoceanography 300 (3–4), 215–225. https://doi.org/10.1016/j.epsl.2010.09.029.

Cheng, H., Sinha, A., Wang, X., Cruz, F. W., & Edwards, R. L. (2012). The global Paleomonsoon as seen through speleothem records from Asia and the Americas. Climate Dynamics, 39(5), 1045–1062. https://doi.org/10.1007/s00382-012-1363-7

Chiang, J. C. H., Biasutti, M., & Battisti, D. S. (2003). Sensitivity of the Atlantic Intertropical Convergence Zone to Last Glacial Maximum boundary conditions. Paleoceanography, 18(4), 1094. https://doi.org/10.1029/2003PA000916

Chiang, J.C.H., Bitz, C.M., (2005). Influence of high latitude ice cover on the marine Intertropical Convergence Zone. Clim Dyn 25, 477–496. doi:10.1007/s00382-005-0040-5

Deplazes, G., Lückge, A., Peterson, L. C., Timmermann, A., Hamann, Y., Hughen, K. A., ... Haug, G. H. (2013). Links between tropical rainfall and North Atlantic climate during the last glacial period. Nature Geosci, 6(3), 213–217. https://doi.org/10.1038/ngeo1712

Franke, J., Paul, A., & Schulz, M. (2008). Modeling variations of marine reservoir ages during the last 45 000 years. Climate of the Past, 4(2), 125–136. https://doi.org/10.5194/cp-4-125-2008

Garcia, H. E., Locarnini, R. A., Boyer, T. P., Antonov, J. I., Baranova, O. K., Zweng, M. M., ... Johnson, D. R. (2014). World Ocean Atlas 2013, Volume 4: Dissolved Inorganic Nutrients (phosphate, nitrate, silicate). In S. Levitus & A. Mishonov (Eds.), NOAA Atlas NESDIS 76 (25 pp.).

Gherardi, J. M., Labeyrie, L., Nave, S., & Francois, R. (2009). Glacial-interglacial circulation changes inferred from record in the North Atlantic region. Paleoceanography, 24, PA2204. https://doi.org/10.1029/2008PA001696

Gregory, J. M., Yin, J., Gregory, J. M., Dixon, K. W., Spelman, M. J., Hurlin, W., ... Weber, S. L. (2006). Investigating the causes of the response of the thermohaline

circulation to past and future climate changes. Journal of Climate, 19(8), 1365–1387. https://doi.org/10.1175/ JCLI3689.1

Hall, I. R., Evans, H. K., & Thornalley, D. J. R. (2011). Deep water flow speed and surface ocean changes in the subtropical North Atlantic during the last deglaciation. Global and Planetary Change, 79(3–4), 255–263. https://doi.org/10.1016/j.gloplacha.2010.12.001

Hemming, S. R. (2004). Heinrich events: Massive late Pleistocene detritus layers of the North Atlantic and their global climate imprint. Reviews of Geophysics, 42(1), RG1005. https://doi.org/10.1029/2003RG000128.

Hodell, D. A., Nicholl, J. A., Bontognali, T. R. R., Danino, S., Dorador, J., Dowdeswell, J. A., ... Röhl, U. (2017). Anatomy of Heinrich layer 1 and its role in the last deglaciation. Paleoceanography, 32, 284–303. https://doi.org/10.1002/2016PA003028

Honisch, B., Allen, K.A., Lea, D.W., Spero, H.J., Eggins, S.M., Arbuszewski, J., deMenocal, P., Rosenthal, Y., Russell, A.D., Elderfield, H., (2013). The influence of salinity on Mg/Ca in planktic foraminifers - evidence from cultures, core-top sediments and complementary delta O-18. Geochim. Cosmochim. Acta 121, 196–213. https://doi.org/10.1016/j.gca.2013.07.028.

Huang, K.-F., Oppo, D. W., & Curry, W. B. (2014). Decreased influence of Antarctic intermediate water in the tropical Atlantic during North Atlantic cold events. Paleoceanography, 389, 200–208. https://doi.org/10.1016/j.epsl.2013.12.037

IPCC, (2013): *Climate Change 2013: The Physical Science Basis. Contribution of Working Group I to the Fifth Assessment Report of the Intergovernmental Panel on Climate Change* [Stocker, T.F., D. Qin, G.-K. Plattner, M. Tignor, S.K. Allen, J., Boschung, A. Nauels, Y. Xia, V. Bex and P.M. Midgley (eds.)]. Cambridge University Press, Cambridge, United Kingdom and New York, NY, USA, 1535 pp.

Jeandel, C. (1993). Concentration and isotopic composition of Nd in the South Atlantic Ocean. Paleoceanography, 117(3–4), 581–591. https:// doi.org/10.1016/0012-821x(93)90104-h

Kageyama, M., Paul, A., Roche, D. M., & Van Meerbeeck, C. J. (2010). Modelling glacial climatic millennial-scale variability related to changes in the Atlantic meridional overturning circulation: A review. Quaternary Science Reviews, 29(21–22), 2931–2956. https://doi.org/10.1016/ j.quascirev.2010.05.029

Kanner, L.C., Burns, S.J., Cheng, H., Edwards, R., Cunningham, S., (2012). High-latitude forcing of the South American summer monsoon during the last glacial. Science 335 (6068), 570–573. https://doi.org/10.1126/science.1213397.

Kostov, Y., Armour, K.C., Marshall, J., (2014). Impact of the Atlantic meridional overturning circulation on ocean heat storage and transient climate change. Geophysical Research Letters 41, 2108–2116. doi:10.1002/2013GL058998@10.1002/(ISSN)1944-8007.GRLCMIP5

Lea, D.W., (2014). Elemental and isotopic proxies of past ocean temperatures. In: Holland, H.D., Turekian, K.K. (Eds.), Treatise on Geochemistry, vol. 8, pp. 373–397.

Lozier, M.S., Roussenov, V., Reed, M.S.C., Williams, R.G., (2010). Opposing decadal changes for the North Atlantic meridional overturning circulation. Nature Geoscience 3, 728–734. doi:10.1038/ngeo947

Lund, D.C., Curry, W.B., (2004). Late Holocene variability in Florida Current surface density: Patterns and possible causes. paleoceanography 19, n/a–n/a. doi:10.1029/2004PA001008

Lund, D.C., Curry, W., (2006). Florida Current surface temperature and salinity variability during the last millennium. paleoceanography 21, n/a–n/a. doi:10.1029/2005PA001218

Lund, D.C., Lynch-Stieglitz, J., Curry, W.B., (2006). Gulf Stream density structure and transport during the past millennium. Nature 444, 601–604. doi:10.1038/nature05277

Lynch-Stieglitz, J., & Fairbanks, R. G. (1994). A conservative tracer for glacial ocean circulation from carbon isotope and palaeo-nutrient measurements in benthic foraminifera. Nature, 369(6478), 308–310. https://doi.org/10.1038/369308a0

Lynch-Stieglitz, J., Curry, W. B., & Slowey, N. (1999). A geostrophic transport estimate for the Florida current from the oxygen isotope composition of benthic foraminifera. Paleoceanography, 14(3), 360–373. https://doi.org/10.1029/1999PA900001

Lynch-Stieglitz, J., Adkins, J. F., Curry, W. B., Dokken, T., Hall, I. R., Herguera, J. C., ... Zahn, R. (2007). Atlantic meridional overturning circulation during the Last Glacial Maximum. Science, 316(5821), 66–69. https://doi.org/10.1126/science.1137127

Lynch-Stieglitz, J., Schmidt, M. W., & Curry, W. B. (2011). Evidence from the Florida Straits for Younger Dryas ocean circulation changes. Paleoceanography, 26, PA1205. https://doi.org/10.1029/2010PA002032

Lynch-Stieglitz, J., Schmidt, M. W., Henry, L. G., & Curry, W. B. (2014). Muted change in Atlantic overturning circulation over some glacial-aged Heinrich events. Nature, 7(2), 144–150. https://doi.org/10.1038/ngeo2045

Lynch-Stieglitz, J., (2017). The Atlantic meridional overturning circulation and abrupt climate change. Annu. Rev. Mar. Sci. 9 (1), 83–104. https://doi.org/10.1146/ annurev- marine- 010816- 060415.

Marchitto, T.M., Broecker, W.S., (2006). Deep water mass geometry in the glacial Atlantic Ocean: a review of constraints from the paleonutrient proxy Cd/Ca. Geochem. Geophys. Geosyst. 7 (12). https://doi.org/10.1029/2006GC001323.

Marchitto, T. M. (2006). Precise multielemental ratios in small foraminiferal samples determined by sector field ICP-MS. Geochemistry, Geophysics, Geosystems, 7(5), Q05P13. https://doi.org/10.1029/2005GC001018

Marchitto, T.M., Bryan, S.P., Curry, W.B., McCorkle, D.C., (2007). Mg/Ca temperature calibration for the benthic foraminifer Cibicidoides pachyderma. Paleoceanography 22, PA1203. https://doi.org/10.1029/2006PA001287.

Marchitto, T.M., Curry, W.B., Lynch-Stieglitz, J., Bryan, S.P., Cobb, K.M., Lund, D.C., (2014). Improved oxygen isotope temperature calibrations for cosmopolitan benthic foraminifera. Geochim. Cosmochim. Acta 130, 1–11. https://doi.org/10.1016/ j.gca.2013.12.034.

Marchitto, T.M., Bryan, S.P., Doss, W., McCulloch, M.T., Montagna, P., (2018). A simple biomineralization model to explain Li, Mg, and Sr incorporation into aragonitic foraminifera and corals. Paleoceanography 481, 20–29. https://doi.org/10.1016/j. epsl.2017.10.022.

Marshall, S. J., & Koutnik, M. R. (2006). Ice sheet action versus reaction: Distinguishing between Heinrich events and Dansgaard-Oeschger cycles in the North Atlantic. Paleoceanography, 21, PA2021. https://doi.org/10.1029/2005PA001247

Marshall, J., Armour, K.C., Scott, J.R., Kostov, Y., Hausmann, U., Ferreira, D., Shepherd, T.G., Bitz, C.M., (2014). The ocean's role in polar climate change: asymmetric Arctic and Antarctic responses to greenhouse gas and ozone forcing. Philosophical Transactions of the Royal Society A: Mathematical, Physical and Engineering Sciences. doi:10.1098/rsta.2013.0040

McManus, J.F., Anderson, R.F., Broecker, W.S., Fleisher, M.Q., Higgins, S.M., (1998). Radiometrically determined sedimentary fluxes in the sub-polar North Atlantic during the last 140,000 years. Paleoceanography 155 (1–2), 29–43. https:// doi.org/10.1016/s0012- 821x(97)00201- x.

McManus, J. F., Francois, R., Gherardi, J. M., Keigwin, L. D., & Brown-Leger, S. (2004). Collapse and rapid resumption of Atlantic meridional circulation linked to deglacial climate changes. Nature, 428(6985), 834–837. https://doi.org/10.1038/nature02494

Mercier, H., Lherminier, P., Sarafanov, A., Gaillard, F., Daniault, N., Desbruyères, D., Falina, A., Ferron, B., Gourcuff, C., Huck, T., Thierry, V., (2015). Variability of the meridional overturning circulation at the Greenland–Portugal OVIDE section from 1993 to 2010. Prog. Oceanogr. 132, 250–261. doi:10.1016/j.pocean.2013.11.001

Mielke, C., Williams, E.F., Baehr, J., (2013). Observed and simulated variability of the AMOC at 26°N and 41°N. Geophysical Research Letters 40, 1159–1164. doi:10.1002/grl.50233

Montagna, P., et al., (2014). Li/Mg systematics in scleractinian corals: calibration of the thermometer. Geochim. Cosmochim. Acta 132, 288–310. https://doi.org/10.1016/j.gca.2014.02.005.

Naafs, B. D. A., Hefter, J., Grützner, J., & Stein, R. (2013). Warming of surface waters in the mid-latitude North Atlantic during Heinrich events. Paleoceanography, 28, 153–163. https://doi.org/10.1029/2012PA002354

NGRIP members, (2004). High-resolution record of Northern Hemisphere climate extending into the last interglacial period. Nat. Geosci. 431, 147–151. https://doi.org/10.1038/nature02805.

Oppo, D.W., Gebbie, G., Huang, K.-F., Curry, W.B., Marchitto, T.M., Pietro, K.R., (2018). Data constraints on glacial Atlantic water mass geometry and properties. Paleoceanogr. Paleoclimatol. https://doi.org/10.1029/2018PA003408.

Palter, J.B., Lozier, M.S., 2008. On the source of Gulf Stream nutrients. J. Geophys. Res., Oceans 113 (C6), 543. https://doi.org/10.1029/2007JC004611.

Parker, A.O., Schmidt, M.W., Chang, P., (2015). Tropical North Atlantic subsurface warming events as a fingerprint for AMOC variability during Marine Isotope Stage 3. Paleoceanography 30 (11), 1425–1436. https://doi.org/10.1002/2015PA002832.

Parsons, L. A., Yin, J., Overpeck, J. T., Stouffer, R. J., & Malyshev, S. (2014). Influence of the Atlantic meridional overturning circulation on the monsoon rainfall and carbon balance of the American tropics. Geophysical Research Letters, 41(1), 146–151. https://doi.org/10.1002/ 2013GL058454

Peterson, L.C., Haug, G.H., Hughen, K.A., Röhl, U., (2000). Rapid changes in the hydrologic cycle of the tropical Atlantic during the last glacial. Science 290 (5498), 1947–1951. https://doi.org/10.1126/science.290.5498.1947.

Piepgras, D. J., & Wasserburg, G. J. (1980). Neodymium isotopic variations in seawater. Paleoceanography, 50(1), 128–138. https://doi.org/ 10.1016/0012-821x(80)90124-7

Piepgras, D. J., & Wasserburg, G. J. (1987). Rare earth element transport in the western North Atlantic inferred from Nd isotopic observations. Geochimica et Cosmochimica Acta, 51(5), 1257–1271. https://doi.org/10.1016/0016-7037(87)90217-1

Poggemann, D.-W., Hathorne, E. C., Nürnberg, D., Frank, M., Bruhn, I., Reißig, S., & Bahr, A. (2017). Rapid deglacial injection of nutrients into the tropical Atlantic via Antarctic Intermediate Water. Paleoceanography, 463, 118–126. https://doi.org/10.1016/j.epsl.2017.01.030

Poggemann, D.W., Nürnberg, D., Hathorne, E.C., Frank, M., Rath, W., Reißig, S., Bahr, A., (2018). Deglacial heat uptake by the Southern Ocean and rapid northward redistribution via Antarctic Intermediate Water. Paleoceanogr. Paleoclimatol. https://doi.org/10.1029/2017PA003284.

Raddatz, J., et al., (2013). Stable Sr-isotope, Sr/Ca, Mg/Ca, Li/Ca and Mg/Li ratios in the scleractinian cold-water coral Lophelia pertusa. Chem. Geol. 352, 143–152. https://doi.org/10.1016/j.chemgeo.2013.06.013.

Rahmstorf, S. (1995). Bifurcations of the Atlantic thermohaline circulation in response to changes in the hydrological cycle. Nature, 378(6553), 145–149. https://doi.org/10.1038/378145a0

Rahmstorf, S. (2002). Ocean circulation and climate during the past 120,000 years. Nature, 419(6903), 207–214. https://doi.org/10.1038/ nature01090

Rahmstorf, S., Box, J.E., Feulner, G., Mann, M.E., Robinson, A., Rutherford, S., Schaffernicht, E.J., (2015b). Exceptional twentieth-century slowdown in Atlantic Ocean overturning circulation. Nature Climate Change 5, 475–480. doi:10.1038/nclimate2554

Rasmussen, S. O., Andersen, K. K., Svensson, A. M., Steffensen, J. P., Vinther, B. M., Clausen, H. B., ... Ruth, U. (2006). A new Greenland ice core chronology for the last glacial termination. Journal of Geophysical Research, 111, D06102. https://doi.org/10.1029/2005JD006079

Reimer, P. J., Baillie, M., Bard, E., Bayliss, A., Beck, J. W., Blackwell, P. G., ... Weyhenmeyer, C. E. (2009). IntCal09 and Marine09 radiocarbon age calibration curves, 0-50,000 years cal BP. Radiocarbon, 17(34), 35–44. https://doi.org/10.3916/C34-2010-02-03

Rodríguez Sanz, L., Mortyn, P. G., Herguera, J. C., & Zahn, R. (2013). Hydrographic changes in the tropical and extratropical Pacific during the last deglaciation. Paleoceanography, 28, 529–538. https://doi.org/10.1002/palo.20049

Roemmich, D., & Wunsch, C. (1985). Two transatlantic sections: Meridional circulation and heat flux in the subtropical North Atlantic Ocean. Deep Sea Research Part A. Oceanographic Research Papers, 32(6), 619–664. https://doi.org/10.1016/0198-0149(85)90070-6

Rooth, C. (1982). Hydrology and ocean circulation. Progress in Oceanography, 11(2), 131–149. https://doi.org/10.1016/0079-6611(82)90006-4 Schmittner, A., & Lund, D. C. (2015). Early deglacial Atlantic overturning decline and its role in atmospheric CO2 rise inferred from carbon isotopes ($\delta^{13}C$). Climate of the Past, 11(2), 135–152. https://doi.org/10.5194/cp-11-135-2015

Roussenov, V., Lozier, M.S., Williams, R.G., Smith, D., (2014). Decadal Evolution of Ocean Thermal Anomalies in the North Atlantic: The Effects of Ekman, Overturning, and Horizontal Transport. http://dx.doi.org/10.1175/JCLI-D-12-00234.1 27, 698–719. doi:10.1175/JCLI-D-12-00234.1

Rühlemann, C., Mulitza, S., Lohmann, G., Paul, A., Prange, M., Wefer, G., (2004). Intermediate depth warming in the tropical Atlantic related to weakened thermohaline circulation: combining paleoclimate data and modeling results for the last deglaciation. Paleoceanography 19 (1). https://doi.org/10.1029/2003PA000948.

Schmidt, M.W., Chang, P., Hertzberg, J.E., Them II, T.R., Ji, L., Otto-Bliesner, B.L., (2012). Impact of abrupt deglacial climate change on tropical Atlantic subsurface temperatures. Proc. Natl. Acad. Sci. 109 (36), 14348–14352. https://doi.org/10.1073/ pnas.1207806109.

Schrag, D.P., Hampt, G., Murray, D.W., (1996). Pore fluid constraints on the temperature and oxygen isotopic composition of the glacial ocean. Science 272 (5270), 1930–1932. https://doi.org/10.1126/science.272.5270.1930.

Schrag, D.P., Adkins, J.F., McIntyre, K., Alexander, J.L., Hodell, D.A., Charles, C.D., McManus, J.F., (2002). The oxygen isotopic composition of seawater during the Last Glacial Maximum. Quat. Sci. Rev. 21 (1–3), 331–342. https://doi.org/10.1016/ s0277- 3791(01)00110- x.

Siddall, M., Stocker, T.F., Clark, P.U., 2009. Constraints on future sea-level rise from past sea-level change. Nat. Geosci. 2, 571–575. https://doi.org/10.1038/ngeo587. Them, T.R., Schmidt, M.W., Lynch-Stieglitz, J., 2015. Millennial-scale tropical atmospheric and Atlantic Ocean circulation change from the Last Glacial Maximum and Marine Isotope Stage 3. Earth Planet. Sci. Lett. 427, 47–56. https://doi.org/10.1016/j.epsl.2015.06.062.

Smeed, D.A., Josey, S.A., Beaulieu, C., Johns, W.E., Moat, B.I., Williams, E.F., Rayner, D., Meinen, C.S., Baringer, M.O., Bryden, H.L., McCarthy, G.D., (2018). The North Atlantic Ocean Is in a State of Reduced Overturning. Geophysical Research Letters 45, 1527–1533. doi:10.1002/2017GL076350

Srokosz, M.A., Bryden, H.L., (2015). Observing the Atlantic Meridional Overturning Circulation yields a decade of inevitable surprises. Science 348, 1255575–1255575. doi:10.1126/science.1255575

Thornalley, D. J. R., Barker, S., Broecker, W. S., Elderfield, H., & McCave, I. N. (2011). The deglacial evolution of North Atlantic Deep Convection. Science, 331(6014), 202–205. https://doi.org/10.1126/science.1196812

Thornalley, D.J.R., Oppo, D.W., Ortega, P., Robson, J.I., Brierley, C.M., Davis, R., Hall, I.R., Moffa-Sanchez, P., Rose, N.L., Spooner, P.T., Yashayaev, I., Keigwin, L.D., (2018). Anomalously weak Labrador Sea convection and Atlantic overturning during the past 150 years. Nature 556, 227–230. doi:10.1038/s41586-018-0007-4

Tulloch, R., Marshall, J., (2012). Exploring Mechanisms of Variability and Predictability of Atlantic Meridional Overturning Circulation in Two Coupled Climate Models. Journal of Climate 25, 4067–4080. doi:10.1175/JCLI-D-11-00460.1

Valley, S., Lynch-Stieglitz, J., Marchitto, T.M., (2017). Timing of deglacial AMOC variability from a high-resolution seawater cadmium reconstruction. Paleoceanography 32 (11), 1195–1203. https://doi.org/10.1002/2017pa003099.

Valley, S.G., Lynch-Stieglitz, J., Marchitto, T.M., (2019). Intermediate water circulation changes in the Florida Straits from a 35 ka record of Mg/Li-derived temperature and Cd/Ca-derived seawater cadmium. Paleoceanography 523, 115692. doi:10.1016/j.epsl.2019.06.032

Vellinga, M., Wood, R.A., (2002). Global Climatic Impacts of a Collapse of the Atlantic Thermohaline Circulation. Climatic Change 54, 251–267. doi:10.1023/A:1016168827653

Waelbroeck, C., et al., (2009). Constraints on the magnitude and patterns of ocean cooling at the Last Glacial Maximum. Nat. Geosci. 2 (2), 127–132. https://doi.org/10.1038/ngeo411.

Wang, Y. J., Cheng, H., Edwards, R. L., An, Z. S., & Wu, J. Y. (2001). A high-resolution absolute-dated late Pleistocene monsoon record from Hulu Cave, China. Science, 294(5550), 2345–2348. https://doi.org/10.1126/science.1064618

Weldeab, S., Friedrich, T., Timmermann, A., Schneider, R.R., (2016). Strong middepth warming and weak radiocarbon imprints in the equatorial Atlantic during

Heinrich 1 and Younger Dryas. Paleoceanography 31 (8), 1070–1082. https://doi.org/10.1002/2016PA002957.

Xie, R. C., Marcantonio, F., & Schmidt, M. W. (2012). Deglacial variability of Antarctic Intermediate Water penetration into the North Atlantic from authigenic neodymium isotope ratios. Paleoceanography, 27, PA3221. https://doi.org/10.1029/2012PA002337

Yu, J., Elderfield, H., (2008). Mg/Ca in the benthic foraminifera Cibicidoides wuellerstorfi and Cibicidoides mundulus: temperature versus carbonate ion saturation. Paleoceanography 276 (1–2), 129–139. https://doi.org/10.1016/j.epsl.2008. 09.015.

Xu, X., Chassignet, E.P., Johns, W.E., Schmitz, W.J., Metzger, E.J., (2014). Intraseasonal to interannual variability of the Atlantic meridional overturning circulation from eddy-resolving simulations and observations. Journal of Geophysical Research: Oceans 119, 5140–5159. doi:10.1002/2014JC009994

Zahn, R., Stuber, A., (2002). Suborbital intermediate water variability inferred from paired benthic foraminiferal Cd/Ca and δ13C in the tropical West Atlantic and linking with North Atlantic climates. Earth Planet. Sci. Lett. 200 (1–2), 191–205. https://doi.org/10.1016/S0012- 821X(02)00613- 1.

Zhang, R., Delworth, T.L., Zhang, R., Delworth, T.L., (2005). Simulated Tropical Response to a Substantial Weakening of the Atlantic Thermohaline Circulation. http://dx.doi.org/10.1175/JCLI3460.1 18, 1853–1860. doi:10.1175/JCLI3460.1

Zhang, W., Wu, J., Wang, Y., Wang, Y., Cheng, H., Kong, X., & Duan, F. (2014). A detailed East Asian monsoon history surrounding the 'Mystery Interval' derived from three Chinese speleothem records. Quaternary Research, 82(01), 154–163. https://doi.org/10.1016/j.yqres.2014.01.010

Zhao, J., Johns, W., (2014). Wind-forced interannual variability of the Atlantic Meridional Overturning Circulation at 26.5°N. Journal of Geophysical Research: Oceans 119, 2403–2419. doi:10.1002/2013JC009407

Zweng, M. M, Reagan, J. R., Antonov, J. I., Locarnini, R. A., Mishonov, A. V., Boyer, T. P., ... Biddle, M. M. (2013). World Ocean Atlas 2013, Volume 2: Salinity. In S. Levitus & A. Mishonov (Eds.), NOAA Atlas NESDIS 74 (39 pp.).